

Annual Review of Earth and Planetary Sciences

An Atlas of Phanerozoic Paleogeographic Maps: The Seas Come In and the Seas Go Out

Christopher R. Scotese

Department of Earth and Planetary Sciences, Northwestern University, Evanston, Illinois 60208,
USA; email: cscotese@gmail.com

Annu. Rev. Earth Planet. Sci. 2021. 49:679–728

First published as a Review in Advance on
March 22, 2021

The *Annual Review of Earth and Planetary Sciences* is
online at earth.annualreviews.org

<https://doi.org/10.1146/annurev-earth-081320-064052>

Copyright © 2021 by Annual Reviews.
All rights reserved

Keywords

Earth history, paleogeography, paleoclimate, paleoceanography, plate tectonics, Pangea, Tethys, Panthalassa

Abstract

Paleogeography is the study of the changing surface of Earth through time. Driven by plate tectonics, the configuration of the continents and ocean basins has been in constant flux. Plate tectonics pushes the land surface upward or pulls it apart, causing its collapse. All the while, the unrelenting forces of climate and weather slowly reduce mountains to sand and mud and redistribute these sediments to the sea. This article reviews the changing paleogeography of the past 750 million years. It describes the broad patterns of Phanerozoic paleogeography as well as many of the specific paleogeographic events that have shaped the modern continents and ocean basins. The focus is on the changing latitudinal distribution of the continents, fluctuations in sea level, the opening and closing of oceanic seaways, mountain building, and how these paleogeographic changes have affected global climate, ocean circulation, and the evolution of life. This review presents an atlas of 114 paleogeographic maps that illustrate how Earth's surface has evolved during the past 750 million years. During that time interval, Earth has witnessed the formation and breakup of two supercontinents: Pannotia and Pangea. The continents have been transformed from low-lying flooded platforms to high-standing land areas crisscrossed by the scars of past continental collisions. Oceans have opened and closed, and then opened again in a seemingly never-ending cycle.

- The changing configuration of the continents and ocean basins during the past 750 million years is illustrated in 114 paleogeographic maps.



CONNECT

www.annualreviews.org

- Download figures
- Navigate cited references
- Keyword search
- Explore related articles
- Share via email or social media

- These maps describe how the surface of Earth has been continually modified by mountain building and erosion.
- The changing paleogeography has affected global climate, ocean circulation, and the evolution of life.
- The data and methods used to produce the maps are described in detail.

1. INTRODUCTION

“The seas come in and the seas go out” is a well-known geological saying. This syllogism is based on abundant geological evidence that areas that are now land were once flooded and, conversely, areas that are now flooded were once above sea level. The Greek philosopher Xenophanes (570–475 BC) observed that petrified shells of clams and oysters could be found high on Mt. Olympus and reasoned that the rock layers that made up the mountain were once under water. Similar observations made in antiquity may also have given rise to the various great flood myths that are shared by numerous ancient religions.

The advance and retreat of the seas is one of the great themes of Earth history. The transgression of the sea that floods the continents is recorded in the three-dimensional array of lithologies that are deposited in deepening environments. The subsequent retreat of the sea, or regression, provides a mirror image of these strata and records the gradual shallowing of depositional environments that often culminates in an unconformity or erosional gap in the rock record (Simmons 2012).

The level of the sea at any instant in time is the result of the combined effects of plate tectonics, mantle dynamics, isostatic loading, and the slow evolution of Earth’s climate from hothouse to icehouse conditions. Sometimes sea level change is local; at other times the effect is global or eustatic. This review presents an atlas of paleogeographic maps for 114 time intervals that illustrate how sea level has fluctuated during the past 600 million years. There is at least one map for each geological stage (**Table 1**), or roughly one map every 5 million years. The following sections describe how the maps were made and present a sampling of the paleogeographic maps in the atlas.

Amadeus Grabau (1924) attributed the first use of the term paleogeography to Robert Etheridge in 1881, although regional paleogeographic maps appear in earlier works [such as Gemmellaro in 1834 (Sicily), Crivelli in 1853 (Italy), Austen in 1856 (England), and Dana in 1863 (North America)]. Schuchert’s 1910 and 1955 atlas, *Paleogeography of North America*, was illustrated by 50 paleogeographic maps describing the flooding of North America by vast epeiric seas from the Cambrian to the Pliocene. The importance of paleogeography with regard to our understanding of the history of Earth was recognized and popularized by Grabau (1924) in his two-volume treatise, *Principles of Stratigraphy*. In the very last paragraph of this monumental work, he concludes, “When the science of Stratigraphy has developed so that its basis is no longer palaeontological, and when the sciences of Lithogenesis, of Orogenesis, and of [Surficial Geology], as well as of Biogenesis, are given their due share in the comprehensive investigation of our [E]arth, then we may hope that Paleogeography, the youthful daughter science of Stratigraphy, will have attained unto that stature which will make it the crowning attraction to the student of Earth History” (Grabau 1924, p. 1147).

2. METHODOLOGY

The paleogeographic maps in this atlas were modified from a set of paleogeographic maps originally published in the PALEOMAP PaleoAtlas for ArcGIS (Scotese 2008a–f). This digital atlas,

Table 1 List of paleogeographic maps

Stratigraphic age
Present-day (Holocene, 0 Ma)
<i>Last Glacial Maximum (Pleistocene, 21 ky)</i>
<i>Early Pliocene (Zanclean, 5 Ma)</i>
Middle–late Miocene (Serravallian and Tortonian, 10 Ma)
<i>Middle Miocene (Langhian, 15 Ma)</i>
<i>Early Miocene (Aquitanian and Burdigalian, 20 Ma)</i>
<i>Late Oligocene (Chattian, 25 Ma)</i>
Early Oligocene (Rupelian, 30 Ma)
<i>Late Eocene (Priabonian, 35 Ma)</i>
<i>Late middle Eocene (Bartonian, 40 Ma)</i>
<i>Early middle Eocene (Lutetian, 45 Ma)</i>
Early Eocene (Ypresian, 50 Ma)
<i>Paleocene–Eocene boundary (Paleocene–Eocene Thermal Maximum, 55 Ma)</i>
<i>Paleocene (Danian and Thanetian, 60 Ma)</i>
<i>Cretaceous–Tertiary boundary (latest Maastrichtian, 65 Ma)</i>
<i>Late Cretaceous (Maastrichtian, 70 Ma)</i>
<i>Late Cretaceous (late Campanian, 75 Ma)</i>
<i>Late Cretaceous (early Campanian, 80 Ma)</i>
<i>Late Cretaceous (Santonian and Coniacian, 85 Ma)</i>
Mid-Cretaceous (Turonian, 90 Ma)
<i>Mid-Cretaceous (Cenomanian, 95 Ma)</i>
<i>Early Cretaceous (late Albian, 100 Ma)</i>
<i>Early Cretaceous (middle Albian, 105 Ma)</i>
<i>Early Cretaceous (early Albian, 110 Ma)</i>
<i>Early Cretaceous (late Aptian, 115.8 Ma)</i>
Early Cretaceous (early Aptian, 120 Ma)
<i>Early Cretaceous (Barremian, 125 Ma)</i>
<i>Early Cretaceous (Hauterivian, 130 Ma)</i>
<i>Early Cretaceous (Valanginian, 135 Ma)</i>
<i>Early Cretaceous (Berriasian, 140 Ma)</i>
<i>Jurassic–Cretaceous boundary (145 Ma)</i>
<i>Late Jurassic (Tithonian, 150 Ma)</i>
<i>Late Jurassic (Kimmeridgian, 155 Ma)</i>
Late Jurassic (Oxfordian, 160 Ma)
<i>Middle Jurassic (Callovian, 165 Ma)</i>
<i>Middle Jurassic (Bajocian and Bathonian, 170 Ma)</i>
<i>Middle Jurassic (Aalenian, 175 Ma)</i>
<i>Early Jurassic (Toarcian, 180 Ma)</i>
<i>Early Jurassic (Pliensbachian, 185 Ma)</i>
<i>Early Jurassic (Sinemurian–Pliensbachian, 190 Ma)</i>
<i>Early Jurassic (Sinemurian, 195 Ma)</i>
Late Triassic (Rhaetian–Hettangian, 200 Ma)
<i>Late Triassic (Rhaetian, 205 Ma)</i>

(Continued)

Table 1 (Continued)

Stratigraphic age
<i>Late Triassic (late Norian, 210 Ma)</i>
<i>Late Triassic (mid-Norian, 215 Ma)</i>
<i>Late Triassic (early Norian, 220 Ma)</i>
<i>Late Triassic (Carnian–Norian 225 Ma)</i>
<i>Late Triassic (Carnian, 230 Ma)</i>
<i>Late Triassic (early Carnian, 235 Ma)</i>
<i>Middle Triassic (Ladinian, 240 Ma)</i>
<i>Middle Triassic (Anisian, 245 Ma)</i>
Permo–Triassic boundary (250 Ma)
<i>Late Permian (Lopingian, 255 Ma)</i>
<i>Late middle Permian (Capitanian, 260 Ma)</i>
<i>Middle Permian (Wordian–Capitanian boundary, 265 Ma)</i>
<i>Middle Permian (Roadian and Wordian, 270 Ma)</i>
<i>Early Permian (late Kungurian, 275 Ma)</i>
<i>Early Permian (early Kungurian, 280 Ma)</i>
<i>Early Permian (Artinskian, 285 Ma)</i>
<i>Early Permian (Sakmarian, 290 Ma)</i>
<i>Early Permian (Asselian, 295 Ma)</i>
<i>Late Pennsylvanian (Gzhelian, 300 Ma)</i>
<i>Late Pennsylvanian (Kasimovian, 305.4 Ma)</i>
<i>Middle Pennsylvanian (Moscovian, 310 Ma)</i>
<i>Early–middle Carboniferous (Baskirian–Moscovian boundary, 315 Ma)</i>
<i>Early Pennsylvanian (Bashkirian, 320 Ma)</i>
<i>Late Mississippian (Serpukhovian, 325 Ma)</i>
<i>Late Mississippian (Visean–Serpukhovian boundary, 330 Ma)</i>
<i>Middle Mississippian (late Visean, 335 Ma)</i>
<i>Middle Mississippian (middle Visean, 340 Ma)</i>
<i>Middle Mississippian (early Visean, 345 Ma)</i>
<i>Early Mississippian (late Tournaisian, 350 Ma)</i>
<i>Early Mississippian (early Tournaisian, 355 Ma)</i>
Devono–Carboniferous boundary (360 Ma)
<i>Late Devonian (middle Famennian, 365 Ma)</i>
<i>Late Devonian (early Famennian, 370 Ma)</i>
<i>Late Devonian (late Frasnian, 375 Ma)</i>
<i>Late Devonian (early Frasnian, 380 Ma)</i>
<i>Middle Devonian (Givetian, 385 Ma)</i>
<i>Middle Devonian (Eifelian, 390 Ma)</i>
<i>Early Devonian (late Emsian, 395 Ma)</i>
<i>Early Devonian (middle Emsian, 400 Ma)</i>
<i>Early Devonian (early Emsian, 405 Ma)</i>
<i>Early Devonian (Pragian, 410 Ma)</i>
<i>Early Devonian (Lochkovian, 415 Ma)</i>
Late Silurian (Pridoli, 420 Ma)

(Continued)

Table 1 (Continued)

Stratigraphic age
<i>Late Silurian (Ludlow, 425 Ma)</i>
<i>Middle Silurian (Wenlock, 430 Ma)</i>
<i>Early Silurian (late Llandovery, 435 Ma)</i>
<i>Early Silurian (early Llandovery, 440 Ma)</i>
<i>Late Ordovician (Hirnantian, 445 Ma)</i>
<i>Late Ordovician (Katian, 450 Ma)</i>
<i>Late Ordovician (Sandbian, 455 Ma)</i>
<i>Middle Ordovician (late Darriwilian, 460 Ma)</i>
<i>Middle Ordovician (early Darriwilian, 465 Ma)</i>
<i>Early Ordovician (Floian–Dapingian boundary, 470 Ma)</i>
<i>Early Ordovician (late early Floian, 475 Ma)</i>
<i>Early Ordovician (Tremadocian, 480 Ma)</i>
<i>Cambro–Ordovician boundary (485 Ma)</i>
<i>Late Cambrian (Jiangshanian, 490 Ma)</i>
<i>Late Cambrian (Pabian, 495 Ma)</i>
<i>Late middle Cambrian (Guzhangian, 500 Ma)</i>
<i>Late middle Cambrian (early Epoch 3, 505 Ma)</i>
<i>Early middle Cambrian (late Epoch 2, 510 Ma)</i>
<i>Early middle Cambrian (middle Epoch 2, 515 Ma)</i>
<i>Early–middle Cambrian boundary (520 Ma)</i>
<i>Early Cambrian (late Terreneuvian, 525 Ma)</i>
<i>Early Cambrian (middle Terreneuvian, 530 Ma)</i>
<i>Early Cambrian (early Terreneuvian, 535 Ma)</i>
<i>Cambrian–Precambrian boundary (540 Ma)</i>
<i>Late Neoproterozoic (middle Ediacaran, 600 Ma)</i>
<i>Late Neoproterozoic (late Cryogenian, 630 Ma)</i>
<i>Middle Neoproterozoic (early Cryogenian, 690 Ma)</i>
<i>Early Neoproterozoic (late Tonian, 750 Ma)</i>

Paleogeographic maps for the time intervals in italics can be viewed in **Supplemental Appendix 2**.

Supplemental Material >

designed for use with geographic information system (GIS) software (ArcMap, ESRI), consisted of ~50 time intervals with paleogeographic, plate tectonic, paleolithological (Boucot et al. 2013), paleoceanographic, and paleoclimatic reconstructions (see sidebar titled What Is a Paleogeographic Map? and **Figure 1**).

WHAT IS A PALEOGEOGRAPHIC MAP?

Before discussing the atlas maps, it is necessary to clear up some of the confusion that surrounds the terms paleogeography and paleogeographic map.

The term paleogeography has sometimes erroneously been used to describe any map that shows the continents in their ancient positions; however, the term should be used only to describe maps that illustrate both the ancient location of the continents and the ancient geography (i.e., the ancient distribution of land and sea) (Markwick 2019; Scotese 2016; Scotese & Schettino 2017; Scotese et al. 1979; Ziegler et al. 1977, 1983, 1985, 1997).

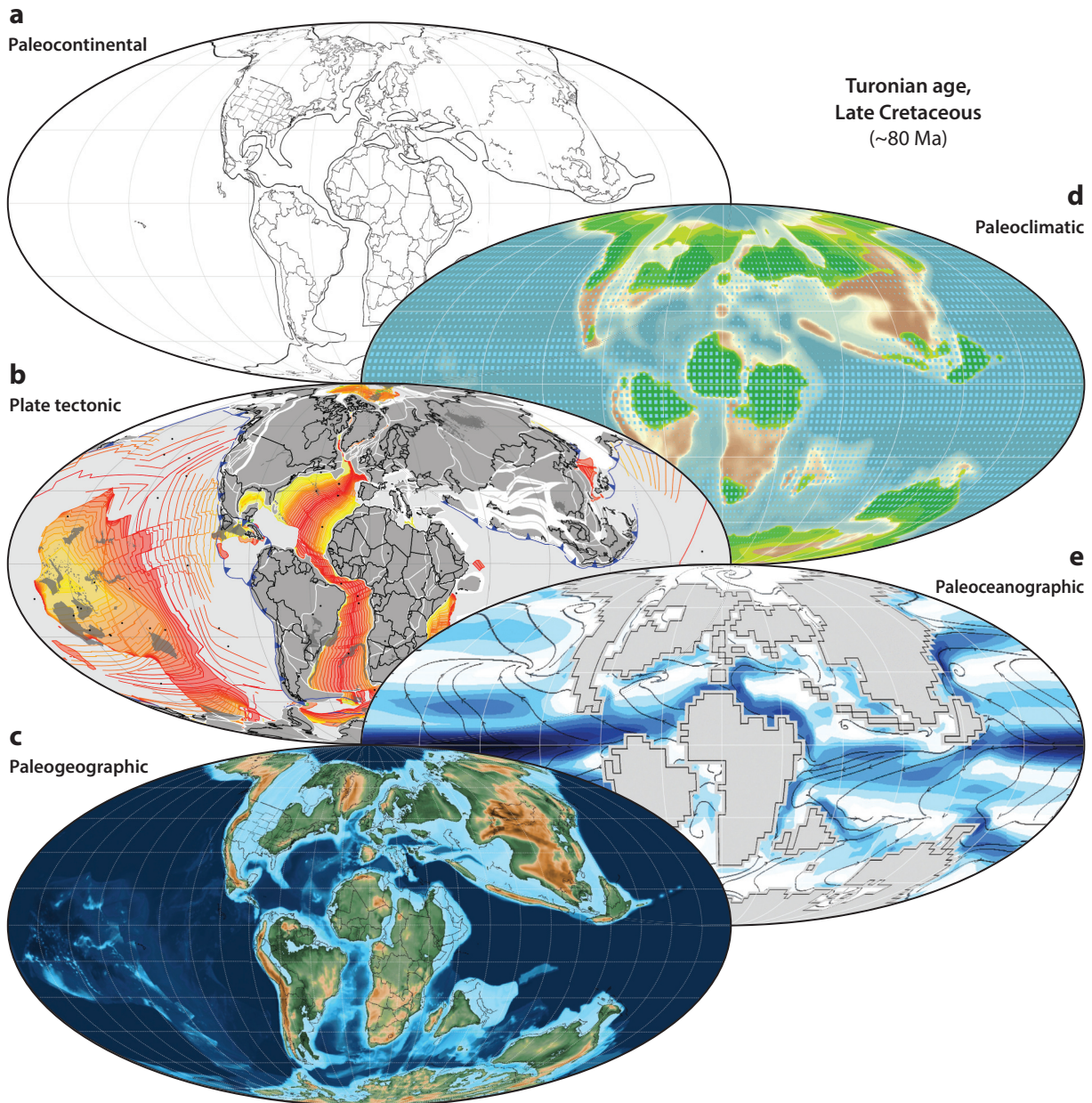


Figure 1

What is a paleogeographic map? (a) Paleocontinental, (b) plate tectonic, (c) paleogeographic, (d) paleoclimatic, and (e) paleoceanographic reconstructions for the Late Cretaceous (Turonian, 80 Ma).

Some definitions are in order:

- A *paleocontinental reconstruction* is a map that shows the modern continents and terranes reconstructed in their ancient locations based on plate tectonic and paleomagnetic information. The black outline shows the boundary between continental and oceanic crust, and

modern coastlines and political boundaries are shown for reference. A paleocontinental reconstruction is the basemap for the other kinds of reconstructions (e.g., Scotese & McKerrow 1990) (**Figure 1a**).

- A *plate tectonic reconstruction* adds ancient active plate tectonic boundaries to a paleocontinental basemap (Scotese 2017; see also Domeier 2016, 2018; Domeier & Torsvik 2014, 2017; Matthews et al. 2016; Müller et al. 1993, 1997, 2008a,b, 2013, 2016; Scotese 2014b, 2017; Seton et al. 2012; Young et al. 2019) (**Figure 1b**).
- A *paleogeographic reconstruction* shows the locations of the ancient shorelines. A complete paleogeographic reconstruction also shows the paleotopography of the continents and paleobathymetry of the ocean basins (**Figure 1c**) and may show the locations of ancient lakes, rivers, deltas, and other geographic features (for an annotated bibliography of key paleogeographic atlases and publications, see **Supplemental Appendix 1**) (for a compilation of recent papers on paleogeography, see Meingold & Şengör 2019).
- A *paleoclimatic reconstruction* adds extra layers illustrating aspects of the ancient climate such as temperature (Scotese & Moore 2014c, Scotese et al. 2021), rainfall (Scotese & Moore 2014b), winds and atmospheric pressure (Scotese & Moore 2014e), and climatic zones (Scotese & Moore 2014d) (see also Haywood et al. 2019, Moore & Scotese 2010, Valdes et al. 2018) (**Figure 1d**).
- A *paleoceanographic reconstruction* adds extra layers illustrating ancient oceanographic features such as surface currents, salinity (Scotese 2014a, Scotese & Moore 2014a), areas of upwelling, and regions of anoxia (Scotese & Moore 2014d) (**Figure 1e**).

Supplemental Material >

The first step in producing a paleogeographic map is to build a global plate tectonic model that describes the evolution of the continents and ocean basins (Scotese 1990, 2001, 2014b, 2016, 2017, 2018; Scotese & Dammrose 2008; Scotese & McKerrow 1990; Scotese & Sager 1989). Once the global plate tectonic framework has been established, paleogeographic maps that describe the ancient distribution of highlands, lowlands, shallow seas, and deep ocean basins can be digitally constructed. The geological lithofacies that define the ancient depositional environments must be mapped to construct an ancient paleogeography. For example, a thick sequence of pure limestones might represent warm, shallow-water environments such as the Bahamas Platform or a vast epeiric sea. Extensive sets of massive, cross-bedded sandstones may once have been wind-blown desert dunes. A terrane composed of andesite and granodiorite may have been a continental arc or Andean mountain range. **Table 2** summarizes the lithofacies and rock types that correspond to the depositional environments that have been used to interpret the ancient topography and bathymetry.

Geologists have been collecting lithologic information and producing lithofacies and paleoenvironmental maps for more than 200 years (Smith 1815). During the late 1970s and early 1980s, the Paleogeographic Atlas Project, under the leadership of A.M. Ziegler in the Department of Geophysical Sciences of the University of Chicago, compiled a database of more than 125,000 lithological and paleoenvironmental records for the Mesozoic and Cenozoic (Ziegler 1975, Ziegler & Scotese 1977, Ziegler et al. 1985). This database was used to produce the paleogeographic maps in this review and has been supplemented by five other lithologic/environmental data sets: a Permian lithofacies database (Rees et al. 2002), a Jurassic lithofacies database (Rees et al. 2000), the Phanerozoic reef database by Kiessling et al. (2002), a database of climatically sensitive lithofacies (Boucot et al. 2013), and environmental information from the Paleobiology Database (Alroy et al. 2008).

Other published sources of paleogeographic maps were consulted when producing the initial set of maps. Some of the key sources include Barrier & Vrielynck (2008), Blakey (2002, 2008), Blakey & Ranney (2018), Bozhko & Khain (1987), Cook (1990), Cook & Bally (1975), Cope et al. (1992), Dercourt et al. (1985, 1993, 2000), Evans et al. (2003), Fensome & Williams (2001),

Table 2 Elevation, environments, and geological evidence

Elevation (m)	Environment(s)	Geological evidence
10,000 to 4,000	Collisional mountains	High-temperature, high-pressure metamorphics
4,000 to 2,000	Andean-type mountains	Andesites/granodiorites in a continental setting
2,000 to 1,000	Island arc volcanoes	Andesites/granodiorites in a marine setting
	Intracontinental rift shoulders	Adjacent fanglomerates
1,000 to 200	Rift valley	Basalts, lake deposits in grabens
	Some forearc ridges	Tectonic mélanges
200 to sea level	Coastal plains	Alluvial complexes
	Lower river systems	Major floodplain complexes
	Delta tops	Swamps and channel sands
Sea level to -50	Inner shelves	Heterogeneous marine sediments
	Reef-dammed shelves	Bahamian-type carbonates
	Delta fronts	Topset silts and sands
-50 to -200	Outer shelves	Fine sediments, most bioproductites
	Some epeiric basins	Fine clastics or carbonates
	Pro-deltas	Foreset silts and proximal turbidites
-200 to -4,000	Continental slope/rise	Slump/contourite facies
	Mid-ocean ridges	Oceanic crust less than 60 million years old
	Pro-delta fans	Bottomset clays and distal turbidites
-4,000 to -6,000	Ocean floors	Pelagic sequences on oceanic crust
-6,000 to -12,000	Ocean trenches	Turbidites on pelagic sequences

Golonka (2000, 2007), Kazmin & Natapov (1998), Kiessling et al. (2002), Ma et al. (2009), Mallory (1972), McCrossan et al. (1964), Ronov et al. (1984, 1989), Schandlmeier & Reynolds (1997), Scotese (1998, 2001, 2004, 2009), Scotese et al. (1979), Şengör & Natal'lin (1996), Şengör et al. (2014a,b), Smith et al. (1994), Stampfli (2000), Stampfli & Borel (2002, 2004), Stampfli & Kozur (2006), Stampfli & Pillevuit (1993), Stampfli et al. (2001, 2013), Ulmishek & Klemme (1990), Veevers (1984, 2000), Vinogradov et al. (1967, 1968a,b, 1969), Wang (1985), Yilmaz et al. (1996), Zheng & Hu (2010), A.M. Ziegler et al. (1977, 1979, 1983, 1985, 1997), P.A. Ziegler (1982, 1988, 1990), P.A. Ziegler et al. (2001), Ziegler & Horvath (1996), and Zonenshain et al. (1990). In addition to these key references, for an annotated bibliography of more than 100 sources of primary paleogeographic information, refer to **Supplemental Appendix 1**. Also, Torsvik & Cocks (2017) provide an excellent summary of the information that goes into making plate tectonic and paleogeographic maps in their book *Earth History and Paleogeography*.

Information from the five lithologic databases was standardized, sorted by time interval, and plotted in the simplified fashion shown in **Figure 2**. These maps show the control points for the paleogeographic interpretations. In these simplified maps, the paleocoastlines weave their way between geologic data indicating marine environments or terrestrial environments. The size of the symbol in **Figure 2** is proportional to the duration of the stratigraphic interval—small symbols are better dated than large symbols. The paleogeographic interpretations were then cross-checked with paleogeographic maps that have been published in numerous regional and global paleogeographic atlases (**Supplemental Appendix 1**).

Lithologic data can be used to map paleogeographic environments only where the rock record is fairly complete. In the many instances where the rock record has been eroded, destroyed by tectonic processes, or covered by younger strata, a second, more interpretive approach was taken to restore the paleogeography. In these instances, the paleoenvironments and paleogeography must

Supplemental Material >

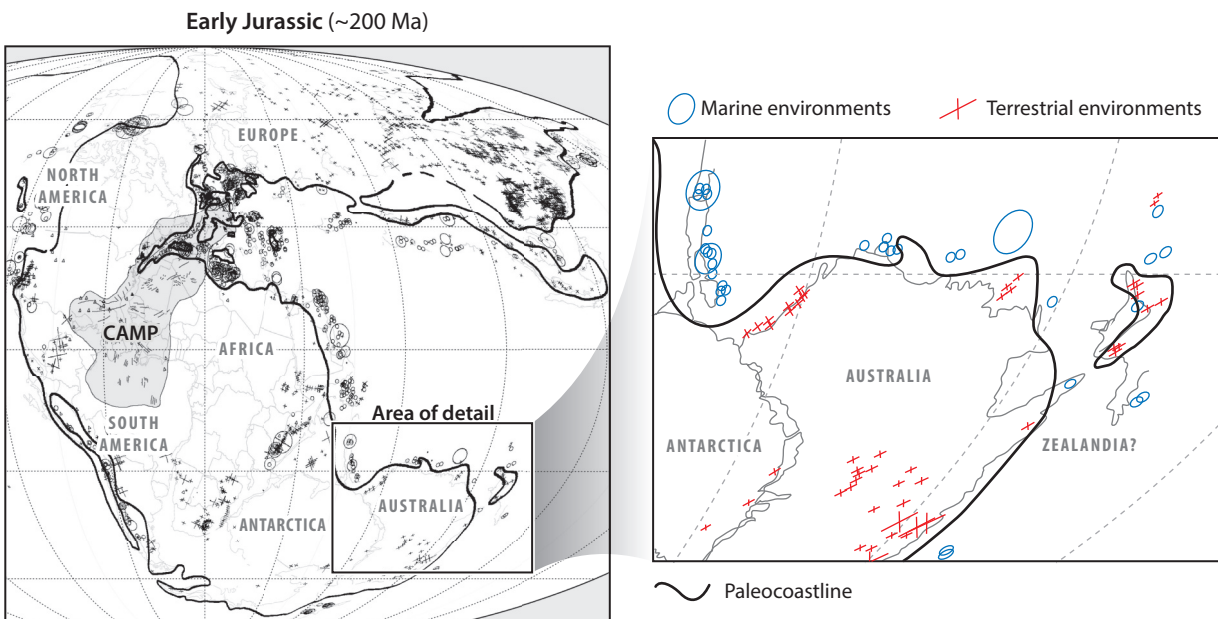


Figure 2

Paleogeographic map for the Early Jurassic (200 Ma) with geologic data used to map the paleocoastline (black line). The size of the symbols is inversely proportional to the precision of the age assignments. The gray-shaded area in the world map is the Central Atlantic Magmatic Province (CAMP). Figure adapted from Scotese & Schettino (2017). Data from GPlates software (Müller et al. 2018) and the Paleobiology Database (Alroy et al. 2008).

be inferred from the tectonic history of a region. The PALEOMAP Global Plate Tectonic Model (Scotese 2016) provides the tectonic framework required to make these inferences and interpretations. The plate tectonic reconstructions (Scotese 2017, 2018) are used to model the expected changes in topography and bathymetry caused by plate tectonic events, such as seafloor spreading, continental rifting, subduction along Andean margins, and continental collision, as well as other isostatic events, such as glacial rebound (Peltier 2004). For example, to produce a paleogeographic map for the Early Cretaceous, young tectonic features, such as recent uplifts or volcanic eruptions (e.g., Mid-African Rift), must be removed or reduced in size, whereas older tectonic features, such as ancient mountain ranges (e.g., Appalachian Mountains), must be restored to their former extent. This approach is similar to the techniques described by Verard et al. (2015), Baatsen et al. (2015), Verard (2019), Markwick (2019), and van der Linden et al. (2020).

In a similar manner, the paleobathymetry of the ocean floor must be restored back through time. Oceanic lithosphere is produced at mid-ocean ridges. As the ocean floor moves away from the spreading ridge, it cools and subsides. In many respects restoring the past bathymetry of the ocean floor is much easier than estimating the elevation of ancient mountain ranges (Rowley & Currie 2006, Rowley & Garzione 2007, Rowley et al. 2001) because as the ocean floor ages, it cools, and as it cools, it sinks. The amount it sinks through time follows a regular mathematical rule that states that the amount of thermal subsidence is inversely proportional to the square root of the age of the oceanic crust (Parsons & Sclater 1977, Sclater et al. 1980). The bathymetry of the ocean floor was unsubsidized to restore the ancient ocean floor to its former depths, using the depth/age relationship originally by Stein & Stein (1992) and later updated by Rowley (2018).

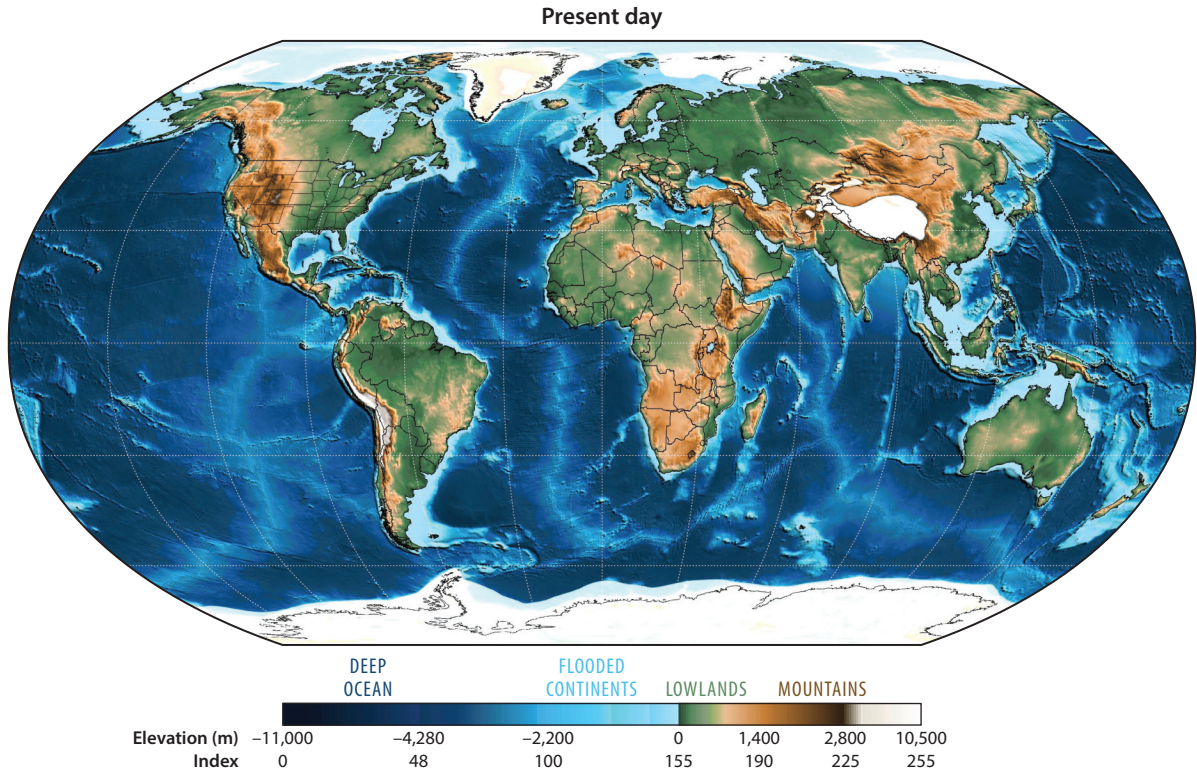


Figure 3

Modern topography and bathymetry color coded by elevation. The color bar along the bottom of the figure lists the colors corresponding to various elevations and the corresponding index color number (0–255).

Once the paleogeography for each time interval was mapped and the corrections to the topography and bathymetry duly noted, this information was converted into a digital representation of paleotopography and paleobathymetry (**Figure 3**). Each paleogeographic map is composed of more than 6 million grid cells that capture digital elevation information at a 10-km × 10-km horizontal resolution and 40-m vertical resolution. This quantitative, paleo-digital elevation model (paleoDEM) allows visualization and analysis of the changing surface of Earth through time using GIS software and other computer modeling techniques.

The process of building a paleoDEM (Scotese 2002) begins with digital topographic and bathymetric data sets of the modern world (Smith & Sandwell 1997), Antarctica (Lythe & Vaughan 2000), and the Arctic (Jakobsson et al. 2004). These topographic and bathymetric data sets were combined into a global data set with 6-min resolution. In the next step, the individual grid cells (latitude, longitude) are rotated back to their paleopositions using the global plate tectonic model of the PALEOMAP Project (Scotese 2016). The resulting map is a reconstruction of present-day bathymetry and topography in a paleolatitudinal and paleolongitudinal framework. However, this reconstructed modern basemap must be modified to reflect ancient topography and bathymetry.

The methodology for building a paleoDEM from geological input is straightforward and uses simple computer graphics techniques. The digital elevation information is converted to an 8-bit color index, where white (index value, 255) represents the highest elevations and black (index value, 0) represents the deepest ocean trenches (**Figure 3**). It is possible to map the

topography and bathymetry at a vertical resolution of 40 m using 256 indexed colors. As illustrated in **Figure 3**, the color index for high mountains is 225 (3,600 m); for lowlands, it is 165 (400 m); for coastal areas, it is 155 (0 m); for shallow seas, it is 150 (−200 m); for deep oceans, it is 75 (−3,200 m); and for the deepest trenches, it is 6 (−10,000). There are fewer index color values for high mountains and deep trenches because these regions represent only a small portion of Earth’s surface.

Increasing or decreasing the elevation of a pixel is simply a matter of changing the index color values until the digital model matches the inferred paleoenvironment. For example, the modern topography for the East African Rift was produced during the past 30 million years. Therefore, on a late Eocene (35 Ma) paleogeographic map of East Africa, the modern topography of the East African Rift must be erased (**Figure 4a**) by digitally editing the mountainous index color values and replacing them with colors that represent lowlands and plains. Conversely, an area that was once an ancient rift valley but has been eroded flat can be rejuvenated by replacing the colors with index colors that represent highlands. **Supplemental Appendix 4** provides a step-by-step set of tutorials describing how to build a paleoDEM using indexed colors.

Recreating ancient topographic features requires a thorough understanding of the overall tectonic evolution of a region as well as a precise knowledge of the tectonic history of every important geographic feature on Earth. One must be able to answer questions such as these: When did this geographic feature first appear? How long did it remain an important geographic feature? When was it eroded? It is also important to note that any changes made on one map must be consistent with the preceding map, as well as with subsequent paleogeographies. That is to say, tectonic features do not suddenly appear and disappear. In fact, the best overall strategy when building the paleotopographic models is to start at the present-day geography and work systematically backward through time, map by map, undoing most recent tectonic events and gradually recreating ancient topographic and bathymetric features.

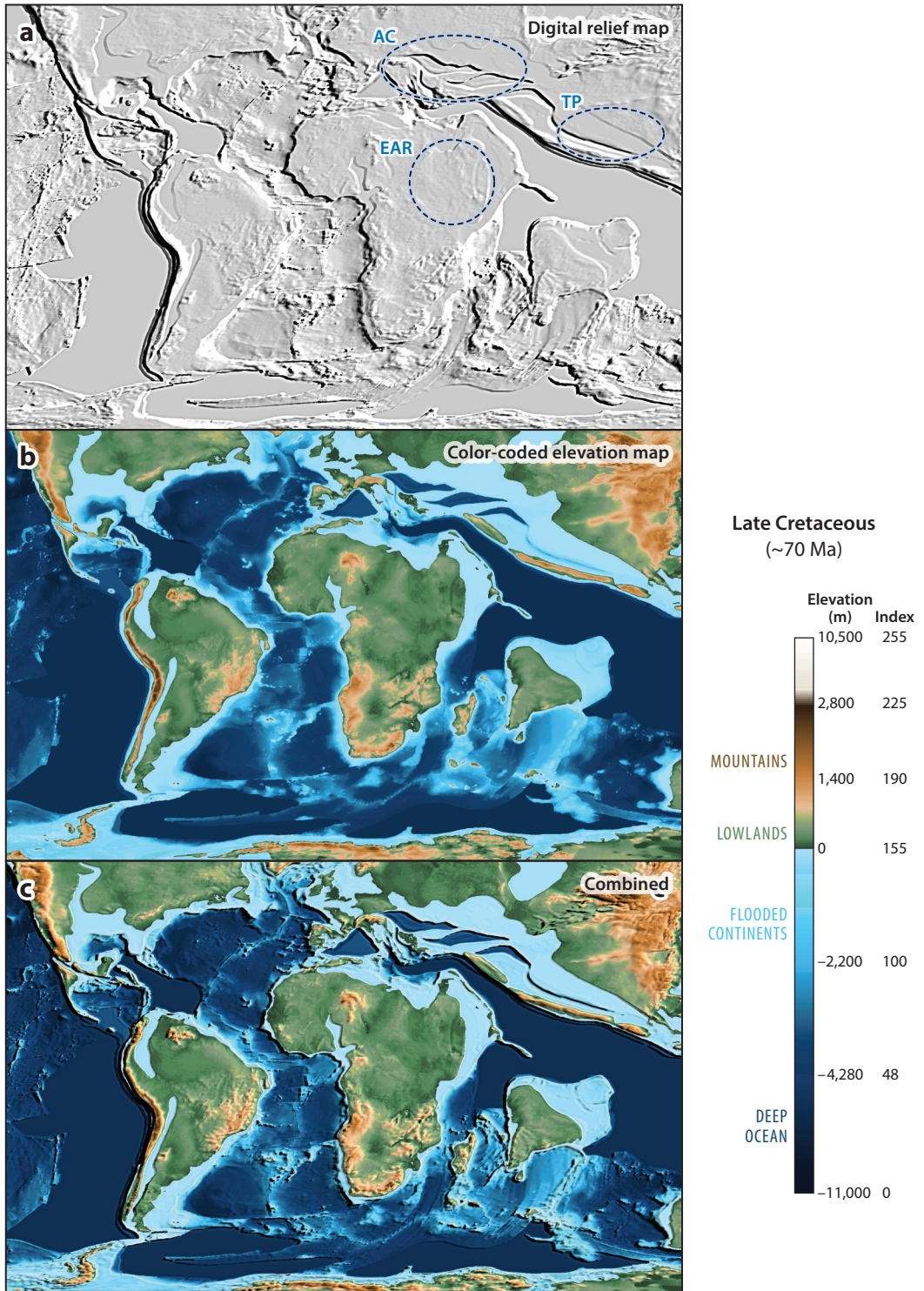
After an indexed color version of the paleoelevations has been built, these indices can be converted back to digital elevation values using this equation: Elevation (m) = (Index Color Value − 155) * 40. The resulting digital elevation file is a global paleotopographic and paleobathymetric paleoDEM for a specific geological time interval (Scotese & Wright 2018).

Because a paleoDEM is a digital model, it can be manipulated in a variety of ways (see the sidebar titled Updating the Paleo-Digital Elevation Models and Paleogeographic Map and **Figure 5**). For example, a paleoDEM can be used to calculate the average elevation of the land surface, the average depth of the ocean floor, the area of the continents flooded by the ocean, or the relative area of continental versus oceanic crust. Through substitution of a modified color look-up table, the digital paleogeography can also be subtly modified to represent eustatic changes in sea level (Algeo & Sleslavinsky 1995; Hallam 1984; Haq & Schutter 2009; Haq et al. 1987; Miller et al. 2005; Müller et al. 2008b; Ross & Ross 1985; Snedden & Liu 2010, 2011; Vail et al. 1977; van der Meer et al. 2017; Verard et al. 2015).

3. CONTENT OF THE PALEOGEOGRAPHIC ATLAS

The Paleogeographic Atlas consists of 114 paleogeographic maps illustrating topography, bathymetry, and polar ice caps (e.g., **Figure 6**). **Table 1** lists the precise chronologic and stratigraphic ages of each paleogeographic map. Each stage map is presented in five map projections: rectilinear, Mollweide, Robinson, north polar (orthographic), and south polar (orthographic). Maps in the rectilinear map projection can be easily mapped onto a sphere or directly imported into GIS programs such as ArcGIS or QGIS. The Mollweide projection is an equal area map projection. The Robinson map projection minimizes the amount of map distortion at all latitudes. The north and south polar projections make it easier to visualize high-latitude regions. The complete

Supplemental Material >



(Caption appears on following page)

Figure 4 (Figure appears on preceding page)

Construction of a global paleogeographic map for 70 Ma. (a) Paleo-digital elevation map with shaded relief. Note that young tectonic features such as the East African Rift (EAR), Tibetan Plateau (TP), and Alps-Caucasus (AC) have been removed (*dashed areas*). (b) Color-coded elevations. (c) Graphical combination of three-dimensional shaded relief and color-coded topography and bathymetry.

UPDATING THE PALEO-DIGITAL ELEVATION MODELS AND PALEOGEOGRAPHIC MAP

The paleodigital elevation model (paleoDEM) is a dynamic representation of paleogeography that can be updated as new information becomes available. In **Figure 5**, a global paleogeographic map for the late Carboniferous (300 Ma) was modified by replacing the default paleogeography for South China with a new interpretation. **Figure 5a** shows a geologic map illustrating lithofacies and depositional environments from Ma et al. (2009). In **Figure 5b** depositional environments are assigned color-coded topography and bathymetry. In **Figure 5c** regional paleogeography for South China is reconstructed to the position it occupied at 300 Ma using GPlates (Müller et al. 2018) and combined with global paleoDEM. **Supplemental Appendix 4** provides a more detailed description of the software tools and procedures used to update the paleoDEMs.

set of more than 500 maps that make up the Paleogeographic Atlas can be found in **Supplemental Appendix 2**. Computer animations illustrating the dynamic evolution of the continents and ocean basins can be found in **Supplemental Appendix 5**.

Supplemental Material >

4. CHRONOLOGICAL REVIEW OF PHANEROZOIC PALEOGEOGRAPHY

This section reviews some of the paleogeographic highlights of the past 600 million years. It outlines the broad patterns of Phanerozoic paleogeography and describes many of the specific paleogeographic events that have shaped the modern continents and ocean basins. The focus of this discussion is on the changing latitudinal distribution of the continents, fluctuations in sea level, the opening and closing of oceanic seaways, mountain building, and how these paleogeographic changes affected global climate, ocean circulation, and the evolution of life. This brief discussion touches on the highlights of Earth's rich and complex paleogeographic history. As we travel back through time, familiar geographic place names are replaced by less familiar paleogeographic references (e.g., Paleotethys, Cimmeria, Laurentia). Index maps (**Figures 7** and **8**) identify these ancient oceans and paleocontinents.

4.1. Paleogeography: Early Ediacaran (600 Ma)

We begin with the formation of the last Precambrian supercontinent, Pannotia (Murphy et al. 2021, Powell & Young 1995) (**Figure 9**). Greater Gondwanaland would be a better name for this latest Precambrian Pangea because at the core of Pannotia is the Paleozoic supercontinent of Gondwanaland (also simply called Gondwana). Gondwana—and hence Pannotia—was assembled when the Congo continent was caught between the colliding northern and southern halves of Rodinia (Hoffman 1991, Scotese 2009) (see the sidebar titled A Note Concerning the Term Pannotia). This series of collisions, known as the Pan-African Orogeny, began ~750 million years ago [initial collision along the Mozambique Belt (Stern 1994)] and may have extended into the early Cambrian (530 Ma) (Meert 2003). The peak in Pan-African orogenesis dates from 610 to 560 Ma (Meert 2003). The immense Pan-African mountain range rivaled the Himalayas in height and covered five times the area of the Tibetan Plateau.

Early Permian (~280 Ma)

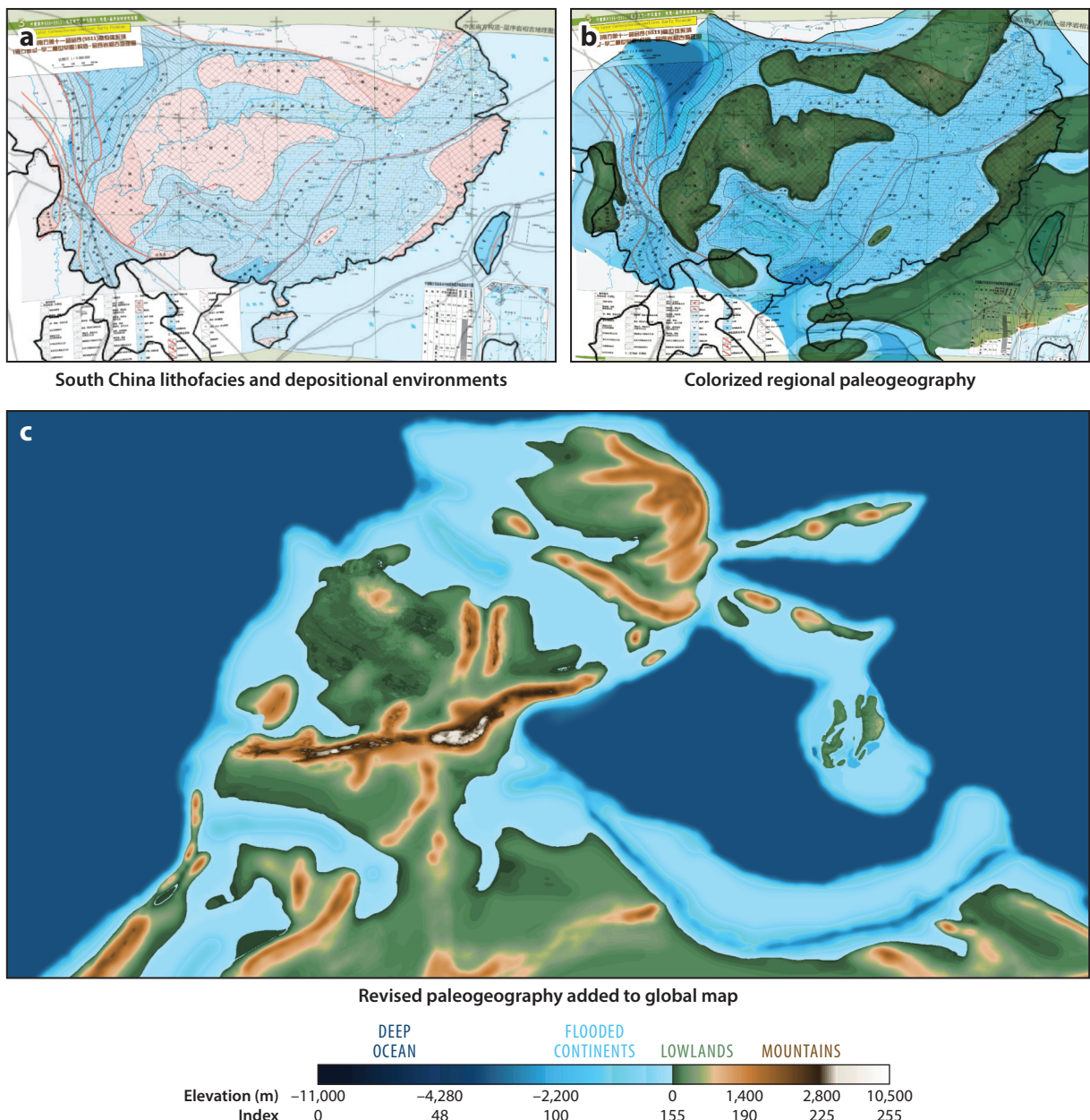


Figure 5

Updating a paleogeographic map using a detailed regional lithofacies map. (a) Lithofacies and depositional environments for South China during the early Permian (280 Ma). (b) Colorized version of the regional paleogeographic map. (c) Adding the revised paleogeography to a global paleogeographic map for the early Permian.

Late Cretaceous (~90 Ma)

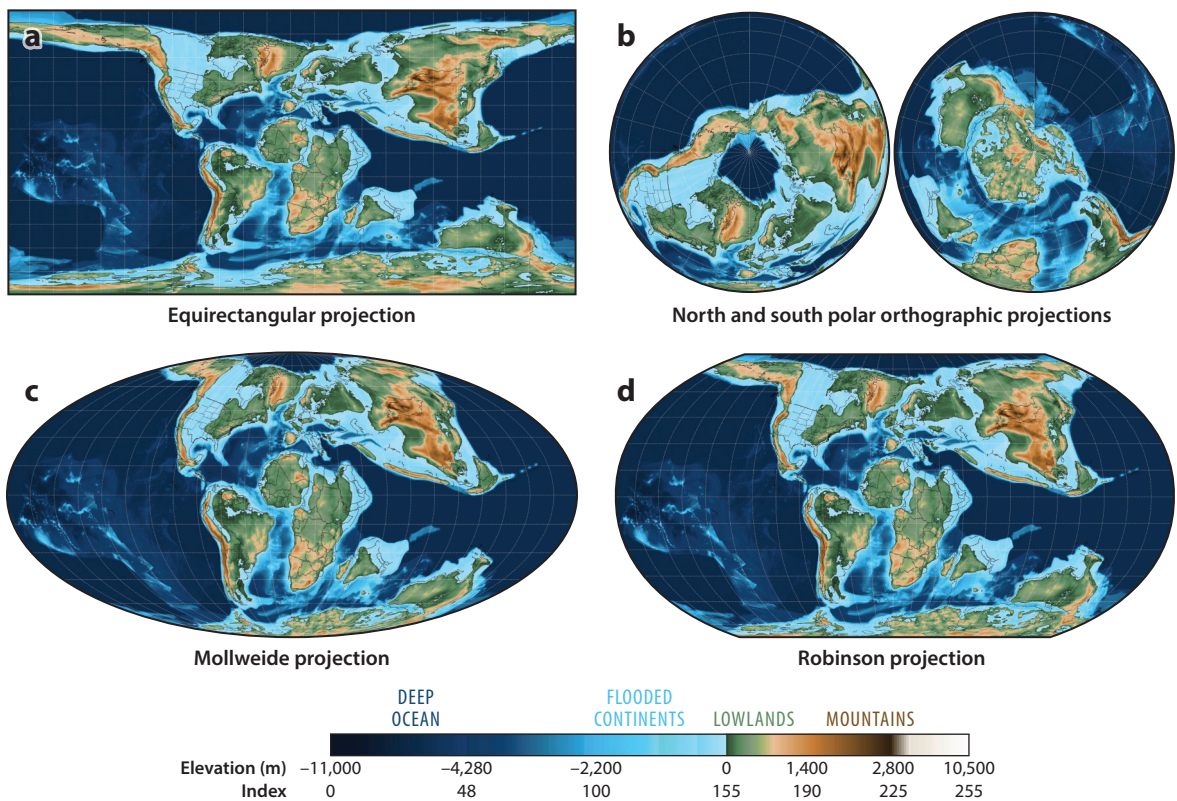


Figure 6

Paleogeographic maps illustrating the configuration of the continents and ocean basins, topography, and bathymetry with modern coastlines and political boundaries. Map projections: (a) equirectangular, (b) north and south polar orthographic, (c) Mollweide, and (d) Robinson. A complete set of paleogeographic reconstructions for more than 100 time intervals can be found in **Supplemental Appendix 2**.

From a climatological point of view, it is significant that much of Pannotia occupied much of the arid southern subtropical belt. The high albedo of this broad desert belt would have reflected sunlight back to space, helping to cool an already cold world. In addition, the rapid erosion of the Pan-African mountains also would have cooled Earth's climate by drawing down the amount of CO₂ in the atmosphere. During the early and middle Cryogenian (720–660 Ma), snow and ice covered the entire globe, giving rise to Snowball Earth (Hoffman et al. 1998). During the latest Precambrian, sea level fell because extensive continental ice sheets sequestered much of the water from the oceans. Low sea level eroded the continents out to the edge of the continental shelf and generated the Great Unconformity, a global erosional hiatus that marks the boundary between the Precambrian and Paleozoic Eras (Keller et al. 2019).

Africa was at the center of Pannotia (**Figure 9**), surrounded by the other Gondwanan continents: Arabia, Madagascar, India, Antarctica, Australia, and South America. The fit of the continents that make up Gondwana is well established (Lawver & Scotese 1987, Scotese et al. 1999, Smith 1999); there is no debate as to the relative positions of these continental blocks. Pannotia also included the early Paleozoic continents of Laurentia (North America), Baltica (Northern Europe), and Siberia.

Supplemental Material >

4.2. Cambro-Ordovician Paleogeography: Tremadocian (480 Ma) and Hirnantian (445 Ma)

Pannotia began to break apart in the latest Precambrian, the same time as the final phases of collision between Africa, Arabia, and parts of Eastern Gondwana (Antarctica, India, and Australia). The breakup of Pannotia formed new ocean basins (e.g., Iapetus Ocean, Rheic Ocean; **Figures 10** and **11**), and sea level rose as the number and length of mid-ocean ridges increased dramatically. Increased seafloor spreading added CO₂ to the atmosphere, and the resulting rise in sea level decreased Earth's albedo, warmed Earth, and ushered in one of the warmest intervals of the Paleozoic, the Cambro-Ordovician Hothouse (**Figure 12**).

Early Paleozoic geography was much different than the geography of the modern world. Panthalassa occupied 90% of the Northern Hemisphere. To fully appreciate the hemispherical asymmetry of the early Paleozoic, one must view this ancient world from both an equatorial and a polar perspective (**Figure 10**). During the Cambro-Ordovician, the Southern Hemisphere was dominated by the supercontinent of Gondwana. Sitting a little lopsided across the South Pole, Gondwana occupied two-thirds of the Southern Hemisphere. The remaining third was taken up by the Rheic and Prototethys Oceans. A patchwork of deep ocean basins, shallow seas, low-lying land areas, and narrow mountain ranges occupied the equatorial region.

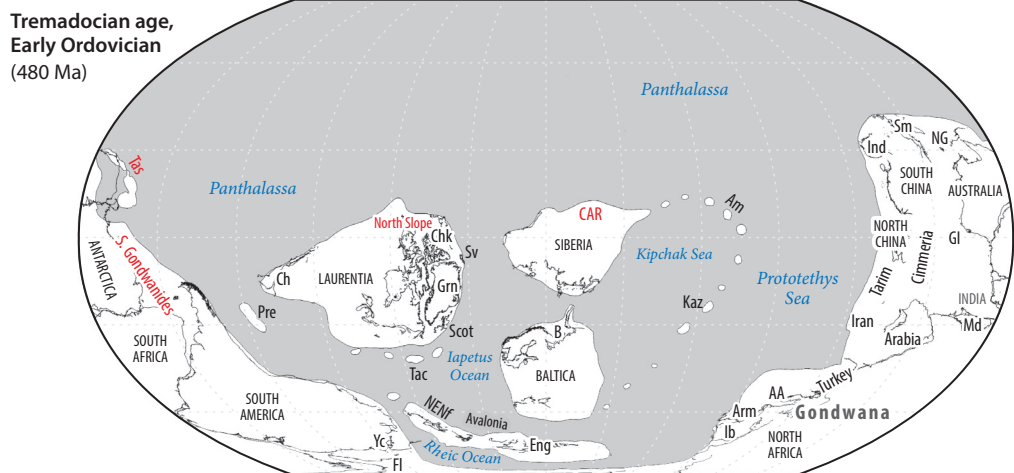
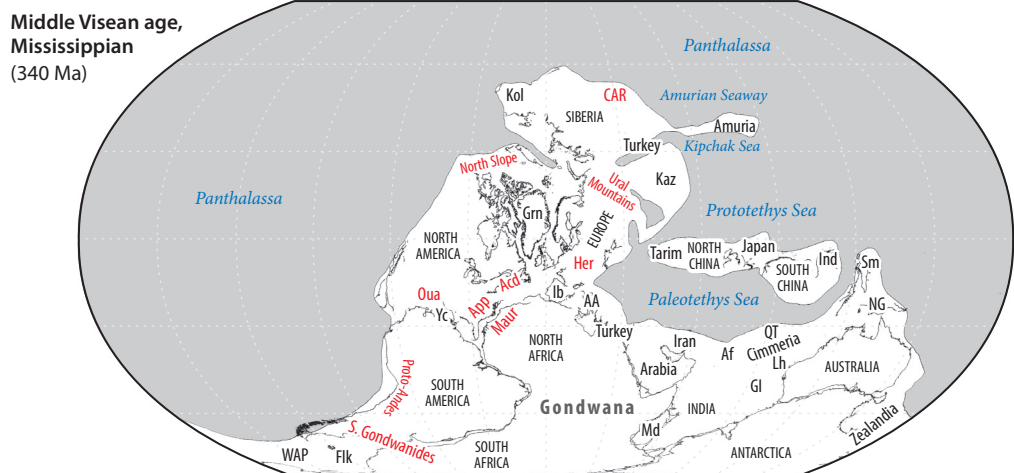
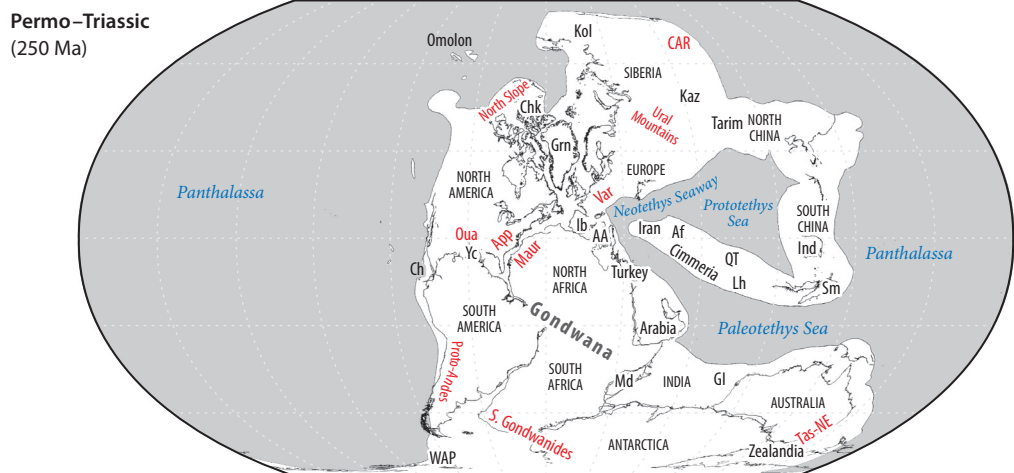
During the early Paleozoic, Australia, South China, and Malaysia occupied the Northern Hemisphere, along with what are now the Arctic regions of Siberia and North America (**Figure 10**). What lay beyond these continents, in the vast northern expanses of the Panthalassa, is still a mystery. Undoubtedly, this ocean floor was once dotted with seamounts and volcanoes. There is biogeographic evidence that the seamounts and islands that originated in the cool northern polar ocean were swept equatorward and incorporated as exotic terranes in the Central Asian mountain ranges of Mongolia, Kazakhstan, and northwestern China [Silurian *Tuvaella* fauna (Rong 1984)].

Oxygen isotope measurements (Trotter et al. 2008) indicate the global temperature gradually began to cool during the Early and Middle Ordovician (**Figure 12**). Paleogeographic changes may have been responsible for this cooling trend. Crowley & Baum (1991) suggested that the growth of the Late Ordovician Gondwana ice cap was facilitated by the combination of increased precipitation and cold temperatures along the northern, ocean-facing margin of Gondwana. Other authors have invoked increased chemical weathering of young mountains (Taconic Ranges) or recently obducted ophiolites that led to a drawdown in atmospheric CO₂, which promoted globally cooler temperatures (Kump & Arthur 1999; Kump et al. 1995, 1999; Swanson-Hysell & Macdonald 2017). This effect may have been enhanced by the evolution of simple, nonvascular land plants (Lenton et al. 2012).

As illustrated in **Figure 12**, one of the most spectacular short-term cooling events of the Phanerozoic took place at the end of the Ordovician [Hirnantian Ice Age, 445–441 Ma (Brenchley et al. 1994, Finnegan et al. 2011, Sheehan 2001, Sheehan & Coorough 1990)] (**Figure 11**). Biostratigraphic (Brenchley et al. 1994) and geochemical data (Finnegan et al. 2011) indicate that the maximum glacial advance was very short lived [less than 1 million years (Ling et al. 2019)] and, therefore, was unlikely to have been due to gradual paleogeographic changes. An alternate explanation invoking a large bolide impact (Khione impact) in the vast Panthalassic Ocean was recently proposed (Scotese et al. 2021).

4.3. Siluro-Devonian Paleogeography: Early Silurian (440 Ma), Late Silurian (420 Ma) and Latest Famennian (360 Ma)

By the late Silurian, the Iapetus Ocean had closed, bringing Laurentia, Baltica, and Avalonia together and creating the northern Appalachian-Caledonian Mountains, which stretched from



(Caption appears on following page)

Figure 7 (Figure appears on preceding page)

Index maps with names of the major paleogeographic features shown in **Figures 4, 10, and 11.** (bottom) Tremadocian (480 Ma), (middle) middle Visean (340 Ma), (top) Permo-Triassic (250 Ma). Red labels indicate mountains. Abbreviations: AA, Apulia-Adria; Acd, Acadian Mountains; Af, Afghanistan; Am, Amuria island arc; App, Appalachian Mountains; Arm, Armorica; B, Barentsia; CAR, Central Asian Ranges; Ch, Chortis; Chk, Chukotka; Eng, England; Fl, Florida; Flk, Falkland Islands; GI, Greater India; Grn, Greenland; Her, Hercynian Mountains; Ib, Iberia; Ind, Indochina; Kaz, Kazakhstan; Kol, Kolyma; Lh, Lhasa; Maur, Mauretanide Mountains; Md, Madagascar; NENf, New England-Newfoundland; NG, New Guinea; NTS, Neotethys Seaway; Oua, Ouachita Mountains; Pre, Precordillera terrane; QT, Qiang Tang; Scot, Scotland; Sm, Sumatra; Sv, Svalbard; Tac, Taconic island arc; Tas, Tasman island arc; Tas-NE, Tasmanide-New England fold belts; Var, Variscan Mountains; WAP, West Antarctic Peninsula; Yc, Yucatan.

southern New York to northern Greenland. By the Late Devonian, the Rheic Ocean between Laurentia and northern South America had also closed (Acadian Orogeny) (**Figure 11**). The Asian parts of Pangea were coming together as the ocean floor continued to be consumed beneath the island arcs of Amuria (Southeast Siberia), Kazakhstan, and the eastern Urals. The location of these terranes, although speculative, is consistent with the gradual amalgamation of central Asia during the late Paleozoic. The Cathaysian continent, made up of Tarim, North China, and South China, is shown in **Figure 11** rifting away from the Indo-Australian margin of Gondwana during the Middle–Late Devonian. The precise position of these terranes is not well constrained by paleomagnetic, tectonic, or paleobiogeographic information. In the Late Devonian, Cathaysia may have been more widely separated from Gondwana than is shown in **Figure 11**.

The paleolatitudinal positions of Laurentia (North America), Baltica (Northern Europe), and Siberia are well supported by paleomagnetic data (Torsvik & Cocks 2017, van der Voo 1993). However, the paleolatitudinal position of Gondwana during the middle Paleozoic is still controversial. Our model locates the South Pole in eastern Argentina, near Rio de Janeiro (Scotese 2017, Torsvik & Cocks 2017), and places the northern coast of Africa at a latitude of 35°S, adjacent to the eastern margin of Laurentia.

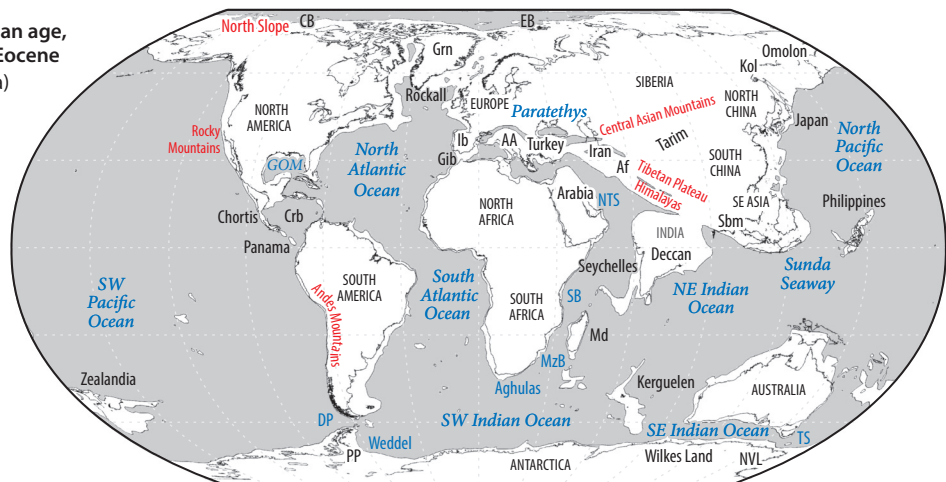
The Early–Middle Devonian collision between southeastern Laurentia and northwestern South America raised an extensive north-south trending mountain range (**Figure 13**). This mountain range isolated brachiopod faunas on either side. Although the Appalachian province and the Rhenish-Bohemian province occupied the same paleolatitudes (~30°S), the Acadian–southern Appalachian Mountains kept them from intermingling. This paleogeographic interpretation also places Morocco, on the northern margin of Gondwana, in warm, subtropical latitudes in the Middle Devonian, consistent with the first occurrence of coral reefs in North Africa (Copper 2002, Copper & Scotese 2003).

During the Middle Devonian, sea level was high and shallow seas flooded the continents. The Middle Devonian (Givetian) recorded one of the highest sea levels of the Phanerozoic [~300 m (Haq & Schutter 2009)]. Sea level briefly fell at the end of the Devonian (latest Famennian) as a result of the growth of a short-lived south polar ice cap (Caputo et al. 2008). One of the most prominent paleogeographic features is the continuous Appalachian–Acadian–Caledonian Mountain range that stretched along northern South America, across the Appalachians, past the British Isles, along eastern Greenland and Scandinavia, and into the Canadian Arctic (**Figure 13**). The lands surrounding these equatorial highlands near Greenland were the home of the first fully terrestrial vertebrates [*Tiktaalik* (Shubin 2008)] and the location of the first coal-producing equatorial rainforests (Boucot et al. 2013).

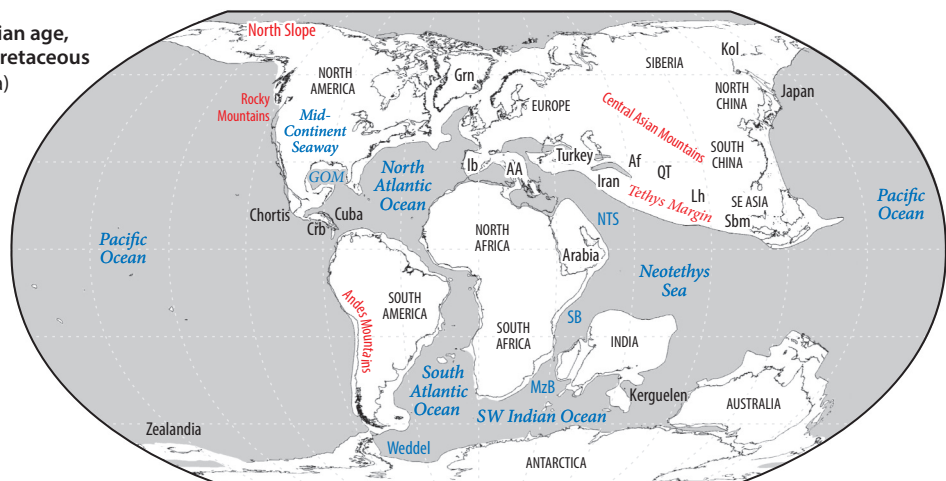
4.4. Carboniferous and Permian Paleogeography: Middle Mississippian (340 Ma) and Permo-Carboniferous Glacial Maximum (295 Ma)

With the exception of a brief warm interval in the early Carboniferous, the late Paleozoic Icehouse chilled the polar regions from the latest Devonian (~360 Ma) to the late Permian (~260 Ma)

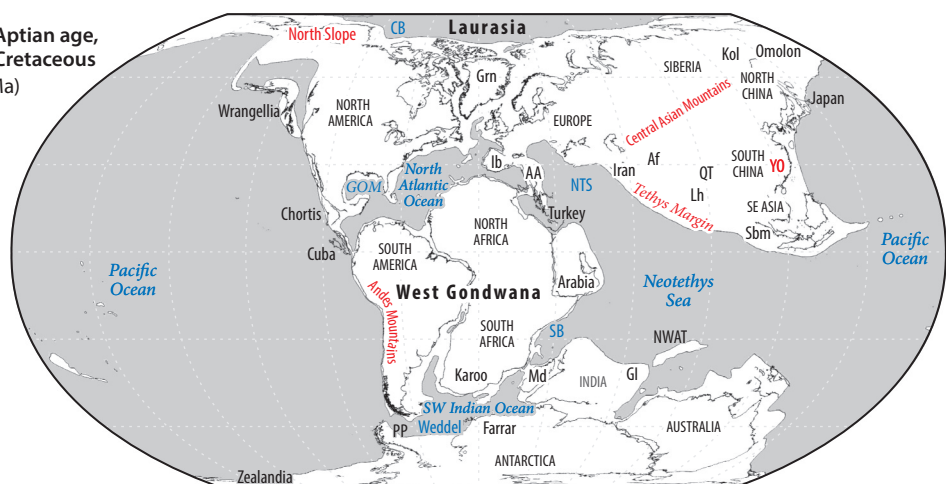
Ypresian age,
early Eocene
(50 Ma)



Turonian age,
Late Cretaceous
(90 Ma)



Early Aptian age,
Early Cretaceous
(120 Ma)



(Caption appears on following page)

Figure 8 (Figure appears on preceding page)

Index maps with names of the major paleogeographic features shown in **Figures 17** and **18**. (*bottom*) Early Aptian (120 Ma), (*middle*) Turonian (90 Ma), (*top*) early Eocene (Ypresian, 50 Ma). Red labels indicate mountains. Abbreviations: AA, Apulia-Adria; Af, Afghanistan; CB, Canada Basin; Crb, Caribbean; DP, Drake Passage; EB, Eurasian Basin; GI, Greater India; Gib, Gibraltar; GOM, Gulf of Mexico; Grn, Greenland; Ib, Iberia; Kol, Kolyma; Lh, Lhasa; Md, Madagascar; MzB, Mozambique Basin; NTS, Neotethys Seaway; NVL, North Victoria Land; NWAT, Northwest Australia terrane; PP, Palmer Peninsula; QT, QiangTang; SB, Somali Basin; Sbm, Sibumasu (Siam-Burma-Malaya-Sumatra); TS, Tasman Straits; YO, Yenshanian Orogeny.

(**Figure 12**). A large south polar ice cap waxed and waned over Gondwana until the late early Permian (~285 Ma), while a smaller ice cap appeared in the northern polar region only at the end of the Permian (~270 Ma). The paleogeography of the Permo-Carboniferous played the principal role in cooling the planet. Three mutually reinforcing factors were in action: intense mountain building along the Equator, vast equatorial rainforests on either side of the Central Pangean Mountains, and the burial of massive amounts of carbon in the form of coal (Boucot et al. 2013).

By the early Carboniferous the continents of Gondwana, Laurentia, Baltica, and Siberia had begun to collide, forming the western core of Pangea. The east-west trending Ouachita Mountains, southern Appalachian Mountains, Hercynian–Variscan Mountains, and Mauretanides marked the collision between northern Gondwana and Laurussia (Laurentia and Baltica). However, in the eastern Pangea, the island arcs of Kazakhstania, Amuria, and the Urals, together with Cathaysia, were still separated by small ocean basins (**Figures 7** and **14**). Young volcanic mountain ranges rose along the sites of future collision zones.

During the Carboniferous and into the early Permian, as Pangea drifted northward, Gondwana rotated counterclockwise over the South Pole. During early Carboniferous (~340 Ma), the South Gondwanan ice cap began to grow in the proto-Andes of Bolivia and western Argentina, which were cold and the recipients of wet, westerly winds (the Roaring Forties). The ice cap expanded across the central Amazon basin, crossed Africa and India in the late Carboniferous, and eventually ended up in southern Australia in the early Permian. During this time interval the South Gondwanan ice cap tripled in size and cooled Earth. In many aspects the climate of the Permo-Carboniferous was similar to our modern icehouse world.

During the Carboniferous and into the early Permian, the Asian parts of Pangea continued to coalesce and the entire supercontinent shifted northward so that the towering Central Pangean Mountains straddled the Equator (**Figure 14**). This equatorial symmetry had two important consequences: Mechanical and chemical weathering accelerated along the length of the Central Pangean Mountains, and dense, broad tropical rainforests covered the flat cratonic regions in North America and Europe that were adjacent to the mountain range. Coincidentally, tropical rainforests covered equatorial South China, and temperate forests covered much of Siberia and southern Gondwana (Boucot et al. 2013).

The weathering of newly exposed igneous and metamorphic rocks in the core of the Central Pangean Mountains provided the chemical constituents (Ca^{++}) required to draw down atmospheric CO_2 (Godderis et al. 2014, 2017; Joshi et al. 2019). The thick growths of newly evolved rainforest flora converted CO_2 into carbon, which was then buried in thick coal seams. These factors led to a steady decrease in the concentration of atmospheric CO_2 , which cooled the planet and led to the growth of a large south polar ice sheet during the middle and late Carboniferous.

The maximum extent of snow and ice occurred during the Permo-Carboniferous Glacial Maximum [~295 Ma (Montañez & Poulsen 2013)] (**Figure 14**). During the late Carboniferous and early Permian (300–280 Ma), Pangea continued to drift northward. As the Central Pangean Ranges crossed the Equator, the mountains increasingly blocked the wet, equatorial easterlies and

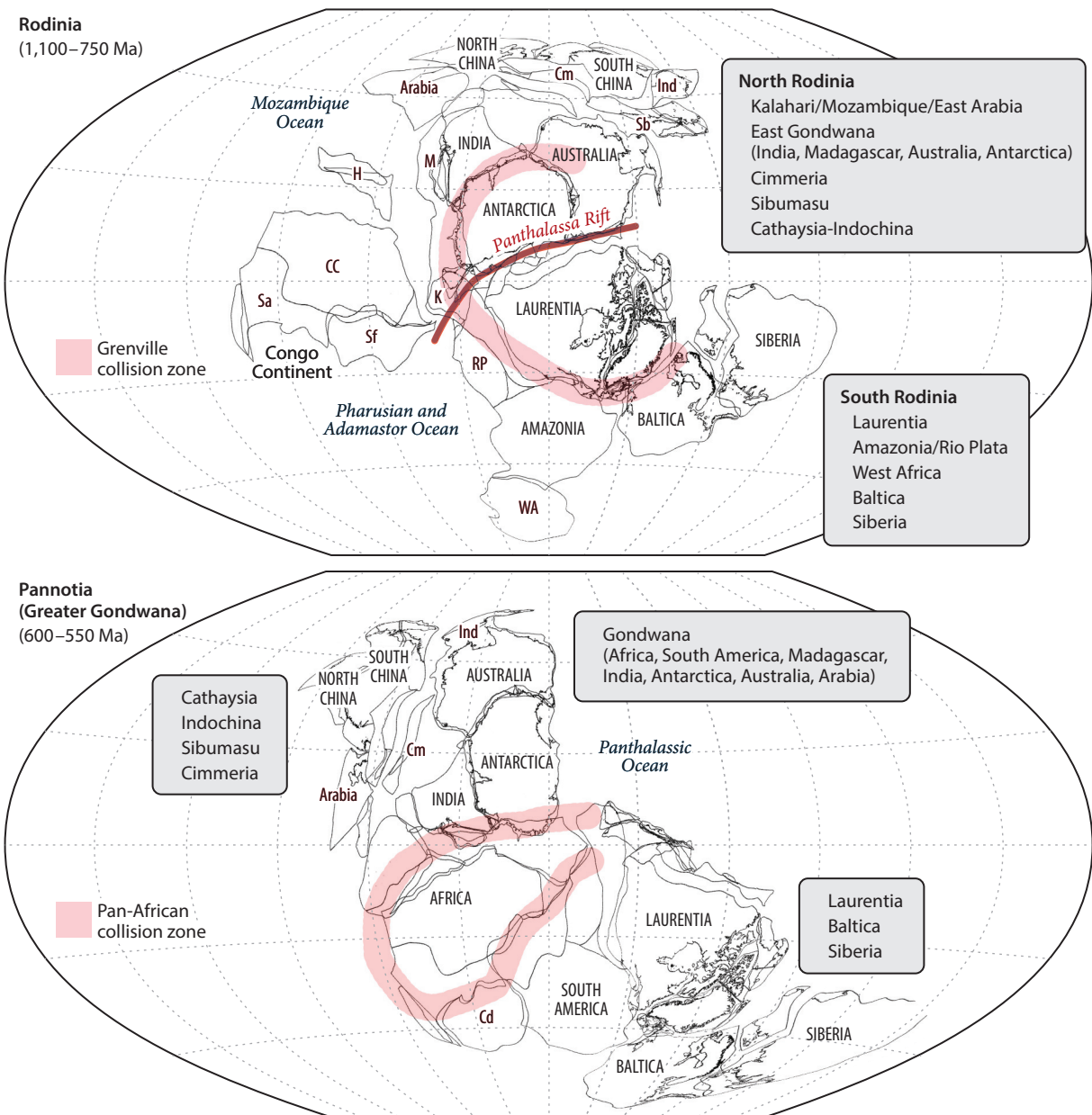


Figure 9

Two late Precambrian supercontinents: Rodinia (1,100–750 Ma) and Pannotia (600–550 Ma). The Pan-African (600 Ma) and Grenville (1,100 Ma) collision zones are shaded pink. Abbreviations: CC, Congo Continent; Cd, Cadomian-Avalonian arc; Cm, Cimmeria; H, Hijaz arc; Ind, Indochina; K, Kalahari craton; M, Madagascar; RP, Rio de la Plata; Sa, Saharan shield; Sb, Sibumasu; Sf, Sao Francisco; WA, West African craton.

A NOTE CONCERNING THE TERM PANNOTIA

In some of the papers discussing Precambrian supercontinents, the term Rodinia (Dalziel 1991, Hoffman 1991, Moores 1991) rather than Pannotia (Powell & Young 1995) is used to describe the Pangea-like configuration that existed at the end of the Precambrian (600–540 million years ago). This is incorrect. Rodinia did not exist 600 million years ago. The term Pannotia should be used for the Precambrian Pangea younger than 700 million years, and the term Rodinia should be used for the Precambrian Pangea older than 700 million years and younger than 1,100 million years (**Figure 9**).

created an arid rain shadow to the north and west of the mountain range. These paleogeographic changes, in combination with low levels of atmospheric CO₂ (Montañez et al. 2007, 2016), stressed the complex tropical ecosystem, and the tropical rainforests shifted from swamp-community floras to seasonally dry vegetation (DiMichele et al. 2009, Richey et al. 2020, Tabor et al. 2013). Other consequences of these paleogeographic changes were that weathering slowed, the concentration of atmospheric CO₂ increased, and global temperatures began to slowly and inexorably increase during the late early Permian (Scotese et al. 2021) (**Figure 14**).

Throughout most of the Carboniferous and early Permian, no landmasses occupied polar latitudes in the Northern Hemisphere. Toward the end of the Permian, however, as Pangea moved northward, Northeast Siberia crossed the polar circle and a small, permanent continental ice cap began to form (Chumakov 1994, Chumakov & Zharkov 2003).

4.5. Permo-Triassic (250 Ma) Paleogeography

At the beginning of the Mesozoic Era, Earth languished in an extreme hothouse world with tropical temperatures exceeding 40°C (**Figure 15**; **Table 3**). It is widely accepted that the great extinction event that occurred at the end of the Permian was caused by extreme global warming triggered by the voluminous eruption of the West Siberian large igneous province (Ernst 2014). The paleogeographic conditions during the late Permian and Early Triassic increased the severity of the Permo-Triassic extinction in two ways: Geographically restricted deep ocean basins were prone to anoxia, and the area of shallow marine habitats was greatly reduced (Snedden & Liu 2010, Verard et al. 2015).

At the end of the Permian (250 Ma), the Paleotethys and Neotethys were largely landlocked oceans (**Figure 14**). The Neotethys narrowed toward its western end, and its eastern end opened into the vast Panthalassa Ocean. The deep waters of the Paleotethys (>200 m), located to the north of Cimmeria (Iran, Afghanistan, QiangTang, Lhasa, and Sibumasu), were completely isolated from Panthalassa. For this reason, it is likely that the deep waters of the Paleotethys were already dysoxic/anoxic prior to the end-Permian extinction. Mixed by wind and wave action, only the surface waters may have been well oxygenated (down to ~100 m). The proposition that the Paleotethys may have been anoxic has given rise to the hypothesis that this so-called deadly ocean was an important contributor to the Permo-Triassic extinction (Şengör & Atayman 2009).

The vast Panthalassa dwarfed both the Paleotethys and Neotethys. A single, linear mid-ocean ridge (Panthalassa Ridge) may have been located near the center of the Panthalassic Ocean basin. Sparse samples of Permo-Triassic deep-water black shales found in a Jurassic accretionary prism in Japan (Isozaki 1997) suggest that parts of the Panthalassic Ocean may also have been anoxic in the late Permian. Preliminary modeling results (Osen et al. 2013) indicate that the deep ocean basin east of the Panthalassic Ridge and west of the Cordilleran subduction zone may have been suboxic or dysoxic.

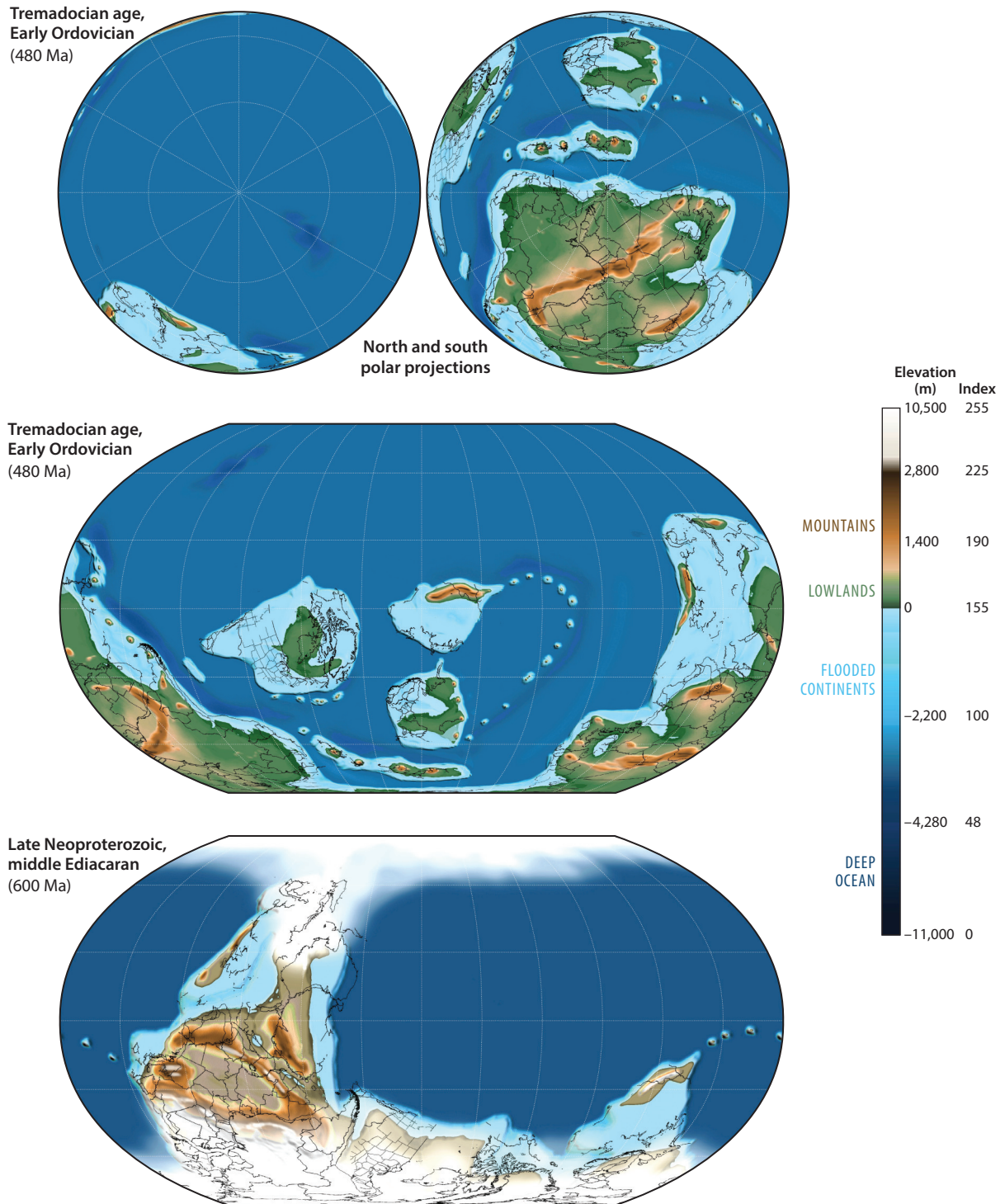


Figure 10

Late Precambrian and Early Ordovician paleogeographic maps.

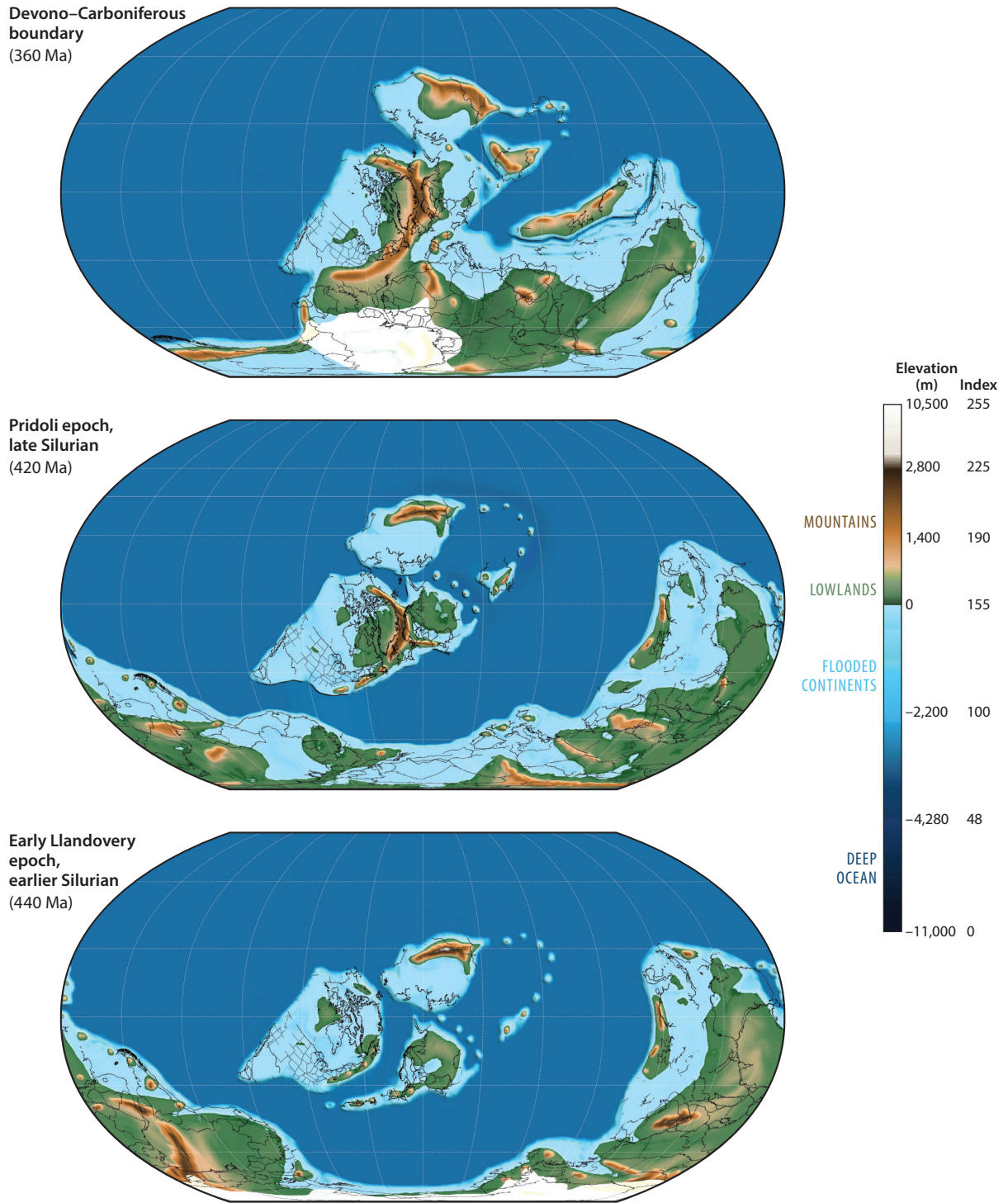


Figure 11

Silurian and Devonian paleogeographic maps.

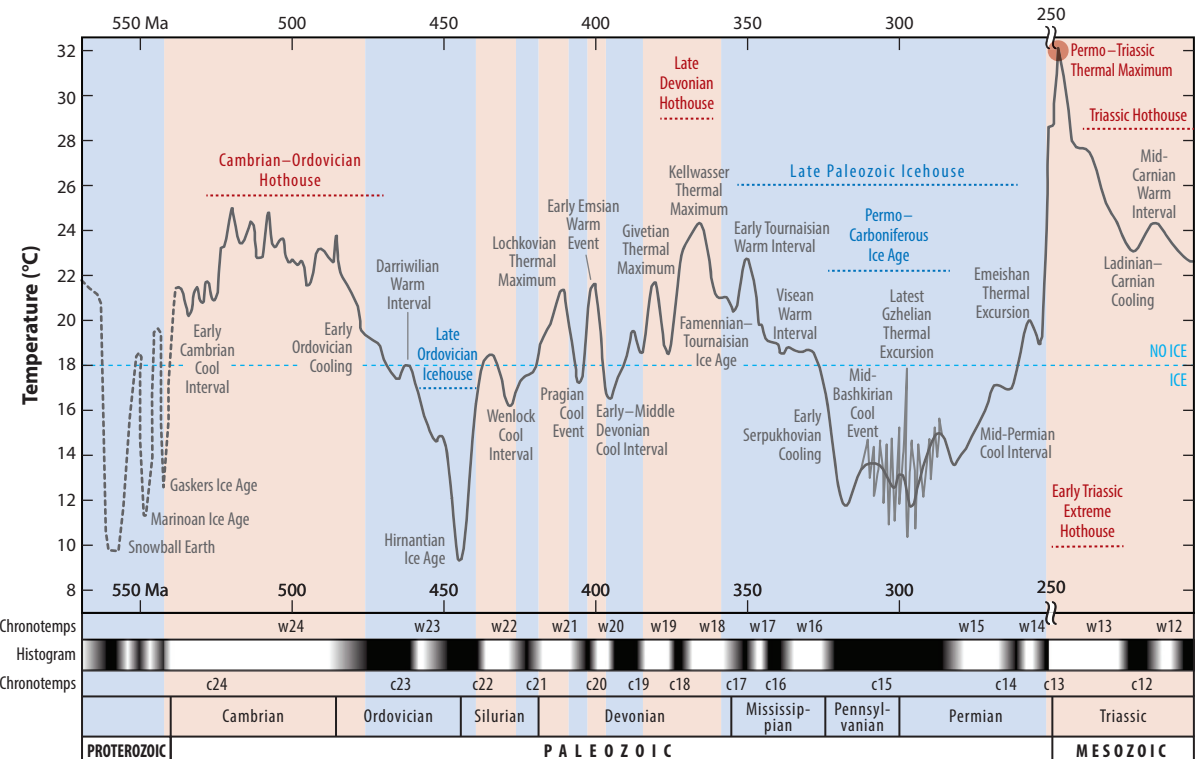


Figure 12

A Paleozoic paleotemperature timescale. Warm time intervals are white; cool time intervals are black. The solid gray line is the Global Average Temperature. Large permanent ice caps are at less than 18°C; no large permanent ice caps are at greater than 18°C. Light gray jagged lines are a schematic representation of more than 50 glacial/interglacial cycles during the Permio-Carboniferous. The timescale is from the International Chronostratigraphic Chart version 2020/01. Refer to Table 3 for more information about each chronotemp. Figure adapted from Scotese et al. (2021).

An additional paleogeographic factor that may have contributed to the severity of the Permo-Triassic extinction was the reduced area of habitable shallow-water shelf environments during the latest Permian. As shown in Figure 16, the area of the globe covered by shallow continental seas decreased steadily during the Carboniferous (~18%), Permian (~15%), and Triassic (~13%) (Kocsis & Scotese 2020). Especially notable is the fact that the area of diverse tropical marine environments decreased rapidly across the late Permian-Early Triassic boundary (Figure 16). This decrease in habitable area may have reduced the diversity of latest Permian faunas and made them more susceptible to extinction [perched fauna (Johnson 1974)].

During the Triassic, Pangea was emergent and the continents were connected by a terrestrial superhighway (Figure 14). The broad, shallow seas of the Paleozoic were gone, replaced by interconnected lands that made it possible for newly evolved reptile groups [e.g., *Lystrosaurus* (Colbert 1982)] to migrate across the globe.

4.6. Jurassic Paleogeography: Earliest Jurassic (200 Ma) and Late Jurassic (160 Ma)

The paleogeographic configuration of the continents during the Jurassic (Figure 17) is the best example of the classic supercontinent Pangea. All the world's landmasses (with the exception of a

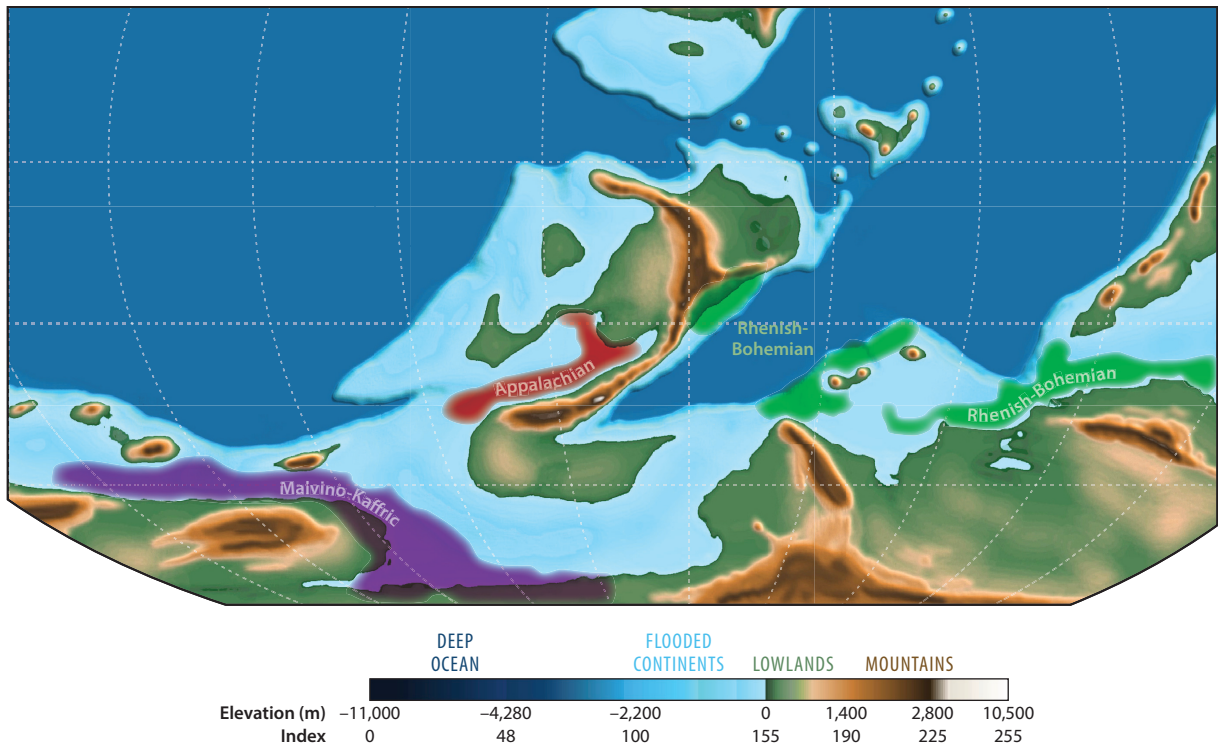


Figure 13

Early Devonian paleobiogeography. The three major fauna provinces are the Appalachian (red), Malvino-Kaffric (purple), and Rhenish-Bohemian (green) (Boucot 1975, Boucot & Gray 1976).

few exotic terranes, such as Wrangellia) were collected in one landmass. The most notable paleogeographic features of the Jurassic Pangea are (*a*) the longitudinal arrangement of Pangea, which stretched from pole to pole; (*b*) the wide, V-shaped Neotethys Sea that separated the northern half of Pangea (Laurasia) from the southern half (Gondwana); (*c*) the broad, shallow cratonic seas that bordered the Neotethys; and (*d*) the open polar oceans.

As illustrated in **Figure 16**, during the Early and Middle Jurassic, the amount of land increased dramatically. The proportion of land in the subtropical arid belt also increased. By modern standards, the climate at low latitudes during the late Early and Middle Jurassic (180–155 Ma) was unbearably hot (**Figure 15**). Average equatorial sea surface temperatures, which were the warmest of the Jurassic, exceeded 30°C, and temperatures in the interior of Pangea often exceeded 40°C (Crowley 1994). The intense summer heating of the large land areas north and south of the Equator strongly deflected the Intertropical Convergence Zone during the summer months. This modification of the basic Hadley Cell circulation pattern has been called megamonsoonal atmospheric circulation (Parrish 1993). Megamonsoons resulted in drier conditions along the Equator and the formation of wide subtropical arid belts.

During the Late Jurassic, global paleogeography began to change drastically. In the Middle Jurassic (~170 Ma), Pangea began to break apart and by the Late Jurassic [155 Ma (**Figure 17**)], narrow ocean basins separated Laurasia (North America and Eurasia), Western Gondwana (Africa, Arabia, and South America), and Eastern Gondwana (Madagascar, India, Antarctica, and Australia). These nascent and highly restricted ocean basins—the Gulf of Mexico, the young North Atlantic

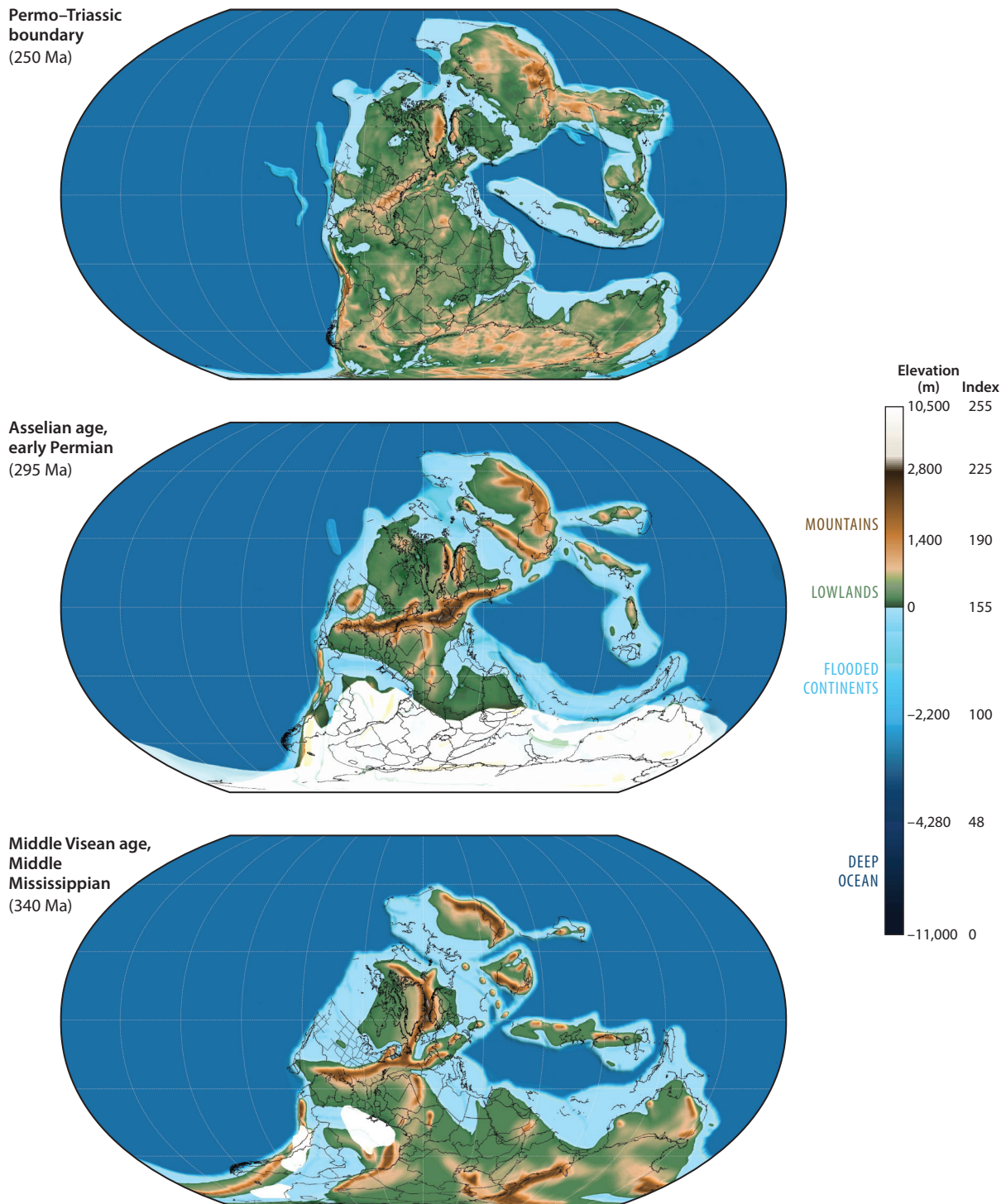


Figure 14

Carboniferous and Permian paleogeographic maps.

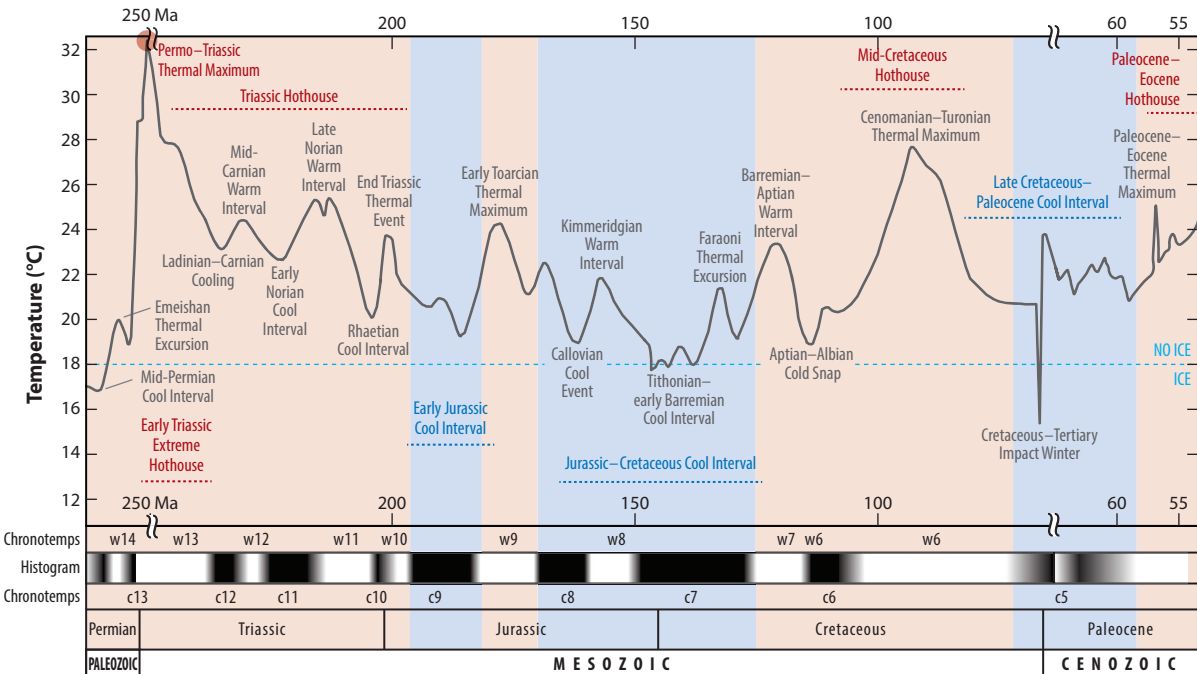


Figure 15

A Mesozoic paleotemperature timescale. Warm time intervals are white; cool time intervals are black. The solid gray line is the Global Average Temperature. Large permanent ice caps are at less than 18°C; no large permanent ice caps are at greater than 18°C. The timescale is from the International Chronostratigraphic Chart version 2020/01. Refer to Table 3 for more information about each chronotemp. Figure adapted from Scotese et al. (2021).

Ocean, and the Somali Basin—provided new sources of moisture for the previously parched interior of subtropical Pangea.

Two other notable paleogeographic features of the Jurassic were the clockwise rotation of the immense Laurasian supercontinent and the open polar oceans during the Middle and Late Jurassic. Rotating clockwise about a pivot point in central Europe, the wet temperate regions of China moved ~1,500 km to the south into the northern arid belt. The highly productive Early Jurassic coal swamps of China were replaced by steppes and deserts with evaporite deposits (Boucot et al. 2013) and a xerophytic flora (Rees et al. 2000). This aridification was enhanced by the rain shadow produced by newly uplifted mountains in southwestern and northeastern China (Xiao et al. 2009). These mountain ranges were the result of latest Triassic–Early Jurassic continental collisions between the Cathaysian, Cimmerian, and Amurian terranes, as well as the initiation of active subduction along the eastern margin of China [Yenshanian Orogeny (Şengör et al. 1993)].

As noted previously, during the Middle and Late Jurassic (175–155 Ma), the polar regions were occupied by deep ocean basins. No continents were present at either the North or South Pole; consequently, ocean currents flowed freely across the poles, and the absence of land at the poles prevented the accumulation of thick continental ice caps. The free circulation of warm ocean waters from lower latitudes helped to keep high latitudes free of ice during the summer months and contributed to generally warmer conditions during most of the Middle and Late Jurassic (Figure 17).

Table 3 Paleozoic, Mesozoic, and Cenozoic paleotemperatures (see Figures 12, 15, and 19)

Chronotemp name	Chronotemp identification number	Age (million years)	Global average temperature (°C)	Δ Tropical temperature (°C)
Post-Anthropogenic Warming (PAW)	W1	-0.005	19.5	3
Modern (2000 CE)	Not applicable	-0.002	14.5	0
Pre-Industrial (1880 CE)	Not applicable	-0.00188	13.8	-0.7
Last Glacial Maximum (LGM)	C1.2	0.02	11	-2
Pliocene Warm Interval (PWI)	W2	4	15.8	1.3
Late Miocene Cool Interval (LMCI)	C2	10	16.3	1
Middle Miocene Warm Interval (MMWI)	W3	15	18.5	2.3
Early Miocene Cool Interval (EMCI)	C3	20	17.3	0.5
Late Oligocene Warm Interval (LOWI)	W4	25	19	1.6
Eocene–Oligocene Rapid Cooling (EORC)	C4.3	33	17.3	-1.5
Middle Eocene Thermal Maximum (METM)	W5.1	42	23.1	3.4
Early Eocene Thermal Maximum (EETM)	W5.6	50	25.1	5.1
Paleocene–Eocene Thermal Maximum (PETM)	W5.9	56	25.2	5
Cretaceous–Tertiary Impact Winter (KTIW)	C5.3	66	8.4	-4.6
Cenomanian–Turonian Thermal Maximum (OAE2)	W6.2	93	28.2	8.2
Aptian–Albian Cold Snap (AACs)	C6	113	19.5	-0.1
Barremian–Aptian Warm Interval (BAWI)	W7	120	23.9	5.3
Tithonian–early Barremian Cool Interval (TEBCI)	C7	145	18.2	-0.8
Kimmeridgian Warm Interval (KWI)	W8	156	22.2	2.8
Middle Jurassic Cool Interval (MJCI)	C8	171	21.5	2.4
Toarcian Warm Interval (TWI)	W9	177	24.6	5.6
Early Jurassic Cool Interval (EJCI)	C9	185	19.6	0
Central Atlantic Magmatic Province (CAMP)	W10.1	200	24.1	4.4
Rhaetian Cool Interval (RCI)	C10	203	20.4	0.7
Late Norian Warm Interval (LNWI)	W11	215	25.7	6.3
Early Norian Cool Interval (ENCI)	C11	223	22.9	2.9
Carnian Pluvial Episode (CPE)	W12.1	230	24.7	4.8
Ladinian–Carnian Cooling (LCC)	C12	240	25.6	5.7
Permo–Triassic Thermal Maximum (PTTM)	W13	250	32.7	13
Latest Permian Cooling (LPC)	C13	254	19.4	0.7
Emeishan Thermal Excursion (ETX)	W14	259	20	2.2
Mid-Permian Cool Interval (MPCI)	C14	265	17.1	0
Artinskian–Kungurian Warming (AKW)	W15	275	15.2	-1.1
Permo–Carboniferous Glacial Maximum (PCGM)	C15.1	295	11.7	-2.3
Latest Gzhelian Thermal Excursion (LGTX)	C15.3	299	13	-0.6
Bashkirian–Moscovian Cool Event (BMCE)	C15.5	312	12.8	-1.7
Mid-Bashkirian Cool Event (MBCE)	C15.6	318	10.9	-3.6
Early Serpukhovian Cooling (ESC)	C15.8	326	17.2	-0.8

(Continued)

Table 3 (*Continued*)

Chronotemp name	Chronotemp identification number	Age (million years)	Global average temperature (°C)	Δ Tropical temperature (°C)
Visean Warm Interval (VWI)	W16	339	19	0.5
Early Mississippian Cooling (EMC)	C16	346	19.2	0.7
Early Tournaisian Warm Interval (ETWI)	W17	355	23	4.6
Famennian–Tournaisian Ice Age (FTIA)	C17	360	20.4	3.4
Kellwasser Thermal Maximum (KTM)	W18.2	373	24	4.9
Early Frasnian Cooling (EFC)	C18	380	18.7	-1
Givetian Thermal Maximum (GTM)	W19	385	21.8	2.4
Early–Middle Devonian Cool Interval (EMDCI)	C19	399	16.8	-1.9
Early Emsian Warm Event (EEWE)	W20	403	21.9	3.6
Pragian Cool Event (PCE)	C20	407	17.5	0
Lochkovian Thermal Maximum (LTM)	W21.1	413	21.6	4.8
Wenlock Cool Interval (WCI)	C21	430	16.4	-1.2
Llandovery Warming (LW)	W22	437	18.5	1.4
Hirnantian Ice Age (HIA)	C22.1	444	9.3	-3.3
Darriwilian Warm Interval (DWI)	W23	463	18.7	1
Early Ordovician Cooling (EOC)	C23	475	19.8	1
Middle–late Cambrian Hothouse (MLCH)	W24	510	24.5	4.5
Early Cambrian Cool Interval (ECCI)	C24	528	23.5	2.7

Table adapted from Scotese et al. (2021).

4.7. Cretaceous Paleogeography: Early Aptian (120 Ma) and Turonian (90 Ma)

The three most prominent paleogeographic features of the Cretaceous were the highstands of sea level (**Figure 16**); the relatively narrow, young ocean basins that separated the fragmented remains of Pangea; and the absence of extensive, high mountain ranges (**Figure 18**). The sea level during the Cenomanian–Turonian highstand (93 Ma, ~200 m) and the early Aptian highstand (120 Ma, ~100 m) was higher than at any other time during the Mesozoic and Cenozoic (Snedden & Liu 2010). Approximately 33% of the continents were covered by shallow seaways (**Figure 16**).

The north-south Midcontinent Seaway divided North America into eastern (Appalachia) and western (Laramidia) landmasses, each with its own distinctive dinosaur fauna (Brownstein 2018). Laramidia was the larger of the two subcontinents, and a proto-Bering Straits land bridge connected Laramidia with northeast Asia, which allowed Late Cretaceous dinosaur faunas to migrate freely between the two landmasses. The Trans-Saharan Seaway isolated northwest Africa from the rest of the continent, and the West Siberian–Caspian Seaway divided Europe from Asia. The Amazon basin, much of western Europe, and Australia–Antarctica were also flooded by the sea.

Continental flooding decreased Earth's albedo and contributed to global warming. More importantly, during times of high sea level, the area of exposed bedrock was reduced, less chemical weathering of igneous and metamorphic rocks took place, and the amount of Ca^{++} transported to the oceans decreased. It comes as no surprise that during these times of high sea level, the drawdown of CO_2 was reduced and the subsequent increase in greenhouse gases warmed the planet (**Figure 15**).

The flooding of vast continental areas resulted in an increase in the diversity and abundance of marine life. The nutrients produced by the death and decay of this biodiversity were transported

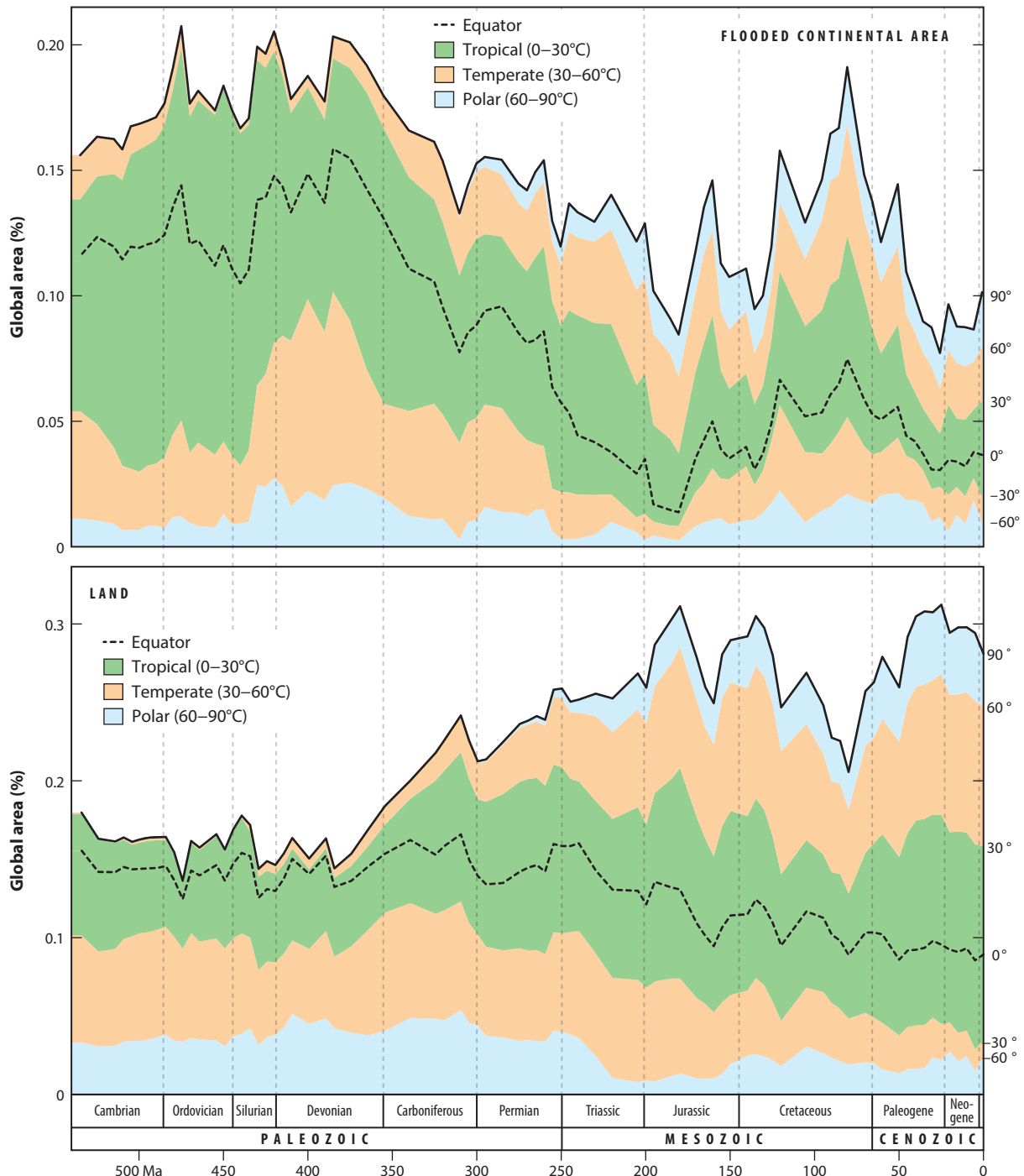


Figure 16

(top) Continental flooding as a percentage of global area (black line). The shaded areas indicate the relative proportion of continental epeiric seas as a function of climatic belt. (bottom) Land as a percentage of global area (black line). The shaded areas indicate the relative proportion of land as a function of climatic belt. Figure adapted from Kocsis & Scotese (2020).

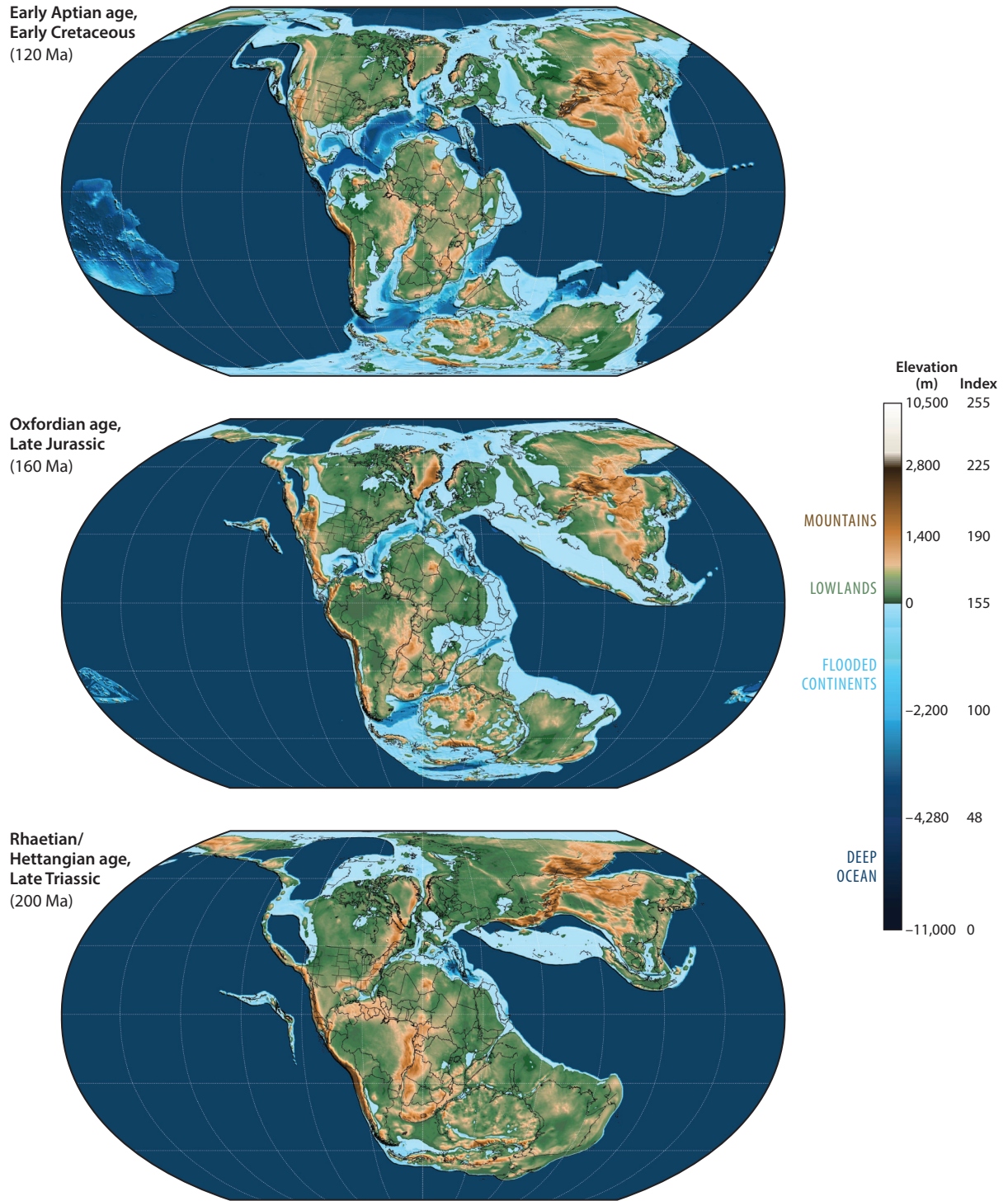


Figure 17

Jurassic and Early Cretaceous paleogeographic maps.

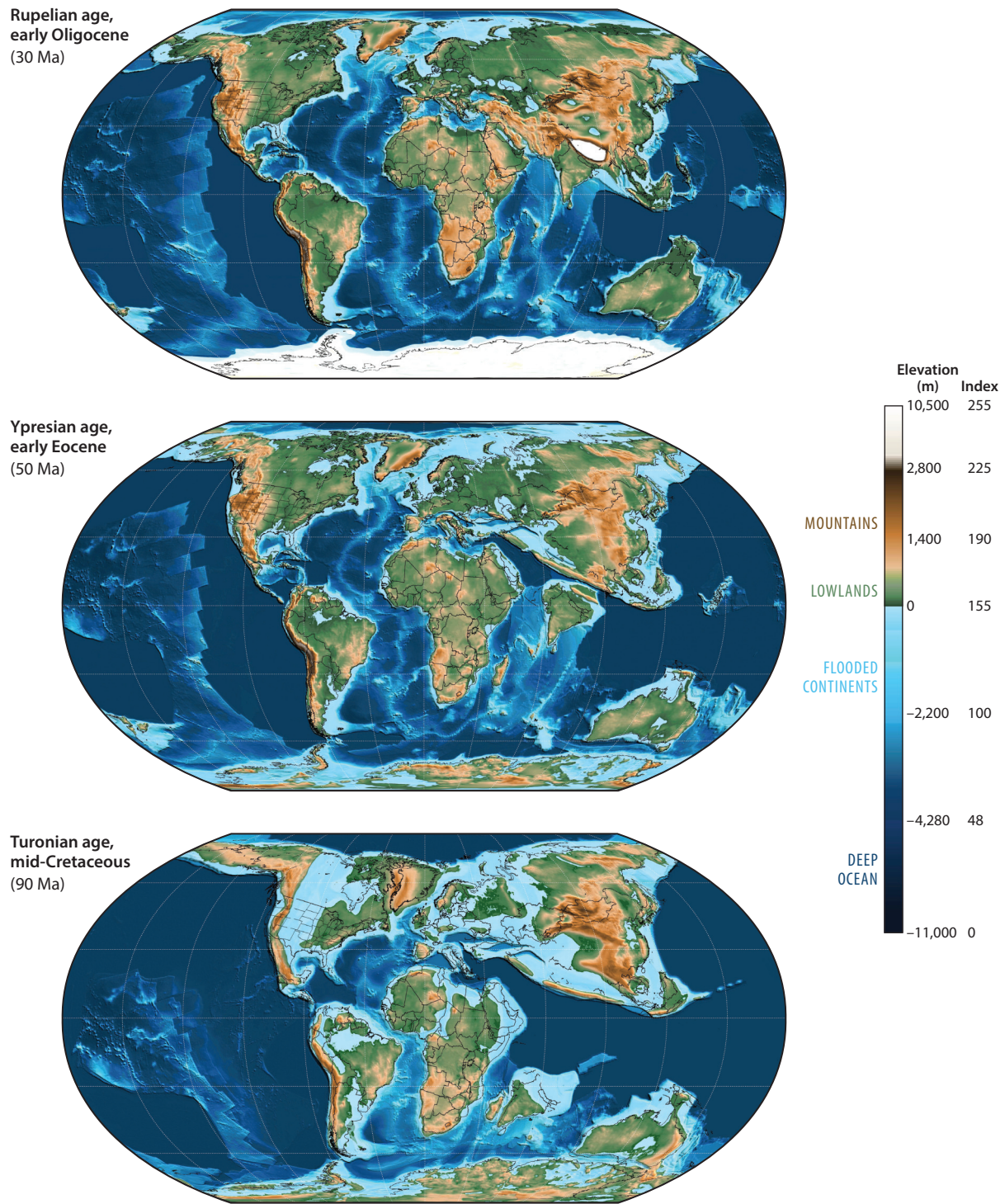


Figure 18

Late Cretaceous and Cenozoic paleogeographic maps.

to the ocean basins, where they promoted greater marine productivity and increased carbon deposition in the deep ocean. The increased productivity depleted the available supply of oxygen in the water column, which led to basin-wide anoxic or dysoxic conditions. Water-column anoxia, in turn, favored the preservation of carbon by inhibiting bacterial decay and carbon recycling. During the Cretaceous, the result was widespread deposition of carbon-rich black shales (Demaison & Moore 1980). For example, the Cenomanian–Turonian highstand is coincident with a widespread deep ocean anoxic event (OAE2, also referred to as the Bonarelli event) (Schlanger & Jenkyns 1976). The early Aptian highstand was coincident with the OAE1a, the Selli–Goguel Thermal Maximum (Erba et al. 2015, Herrle et al. 2015). Deep ocean anoxia and the deposition of widespread black shales were further promoted by the fact that the modern ocean basins (North and South Atlantic, the southwestern Indian Ocean, and Weddell Sea) were less than half their modern width. Ringed by continents, the restricted deep waters in these ocean basins could not flow freely and mix with better-oxygenated deep waters from the surrounding oceans.

Although sea level was high during the Cretaceous, the continents stood relatively low (Hay 2017). The most prominent highlands were the Rocky Mountains, the Canadian Rockies, and the Karoo–Farrar flood basalt plateaus of South Africa and Antarctica.

Many of the Cretaceous highlands were residual uplifts associated with Paleozoic collisions (Caledonides, Appalachians, Hercynides, Urals). The thermal effects associated with the formation of new ocean basins produced uplifted margins on either side of the South Atlantic (145–110 Ma), between Antarctica and India (125–115 Ma), along the margins of the North Atlantic (100–55 Ma), and in west-central India (Deccan Traps, 66–65 Ma).

Convergent margins with a long history of subduction produced Andean-type mountains and continental island arcs along the circum-Pacific margin and along the northern margin of the Tethys. Although there were no major continent-continent collisions during the Cretaceous, several exotic terranes and small continents were accreted along active, convergent margins. These continental collisions included the collision of south-central Asia (North and South China plus Southeast Asia) with southeastern Siberia (130–110 Ma), the collision of Omolon and Kolyma with Northeast Siberia (~115 Ma), the arrival of Wrangellia along the western margin of North America (~110 Ma), and the beginnings of the collision of Apulia and Adria with the southern margin of Europe to form the Alps (70–50 Ma).

4.8. Cenozoic Paleogeography: Early Eocene (Ypresian, 50 Ma) and Early Oligocene (Rupelian, 30 Ma)

The paleogeography of the Cenozoic looks familiar: Six large continental landmasses were separated by widening ocean basins, 60% of Earth's land area was located in the Northern Hemisphere, and a hemisphere-wide ocean covered the remainder of the globe. Although the early Eocene continents have a familiar look (**Figure 18**), there are a few paleogeographic differences worth noting. Australia was farther south, and only a narrow seaway separated it from Antarctica. India, although in the same location that it occupies today, was just beginning to collide with Asia. The southern margin of Asia was undeformed, and the distance between the Himalayas and the Tarim Basin was twice as wide as it is today (3,000 km versus 1,500 km).

With regard to the oceans, the Eocene world was subtly different from the modern world. The South Atlantic and the North Atlantic were 20% narrower than today's oceans. The far North Atlantic, between Greenland and Europe, was just beginning to open. Although some ocean floor had formed in both the Greenland–Norwegian basin and the Eurasian basin, Greenland and Northern Europe were still connected by shallow seas. During lowstands in sea level, it would have been possible to walk from Europe to North America. The North Greenland–Svalbard land bridge and the Southeast Greenland–Iceland–Northern Europe land bridge were the preferred routes for early

mammals migrating between Europe and North America (McKenna 1973). On the other side of the globe, the Pacific Ocean was slightly larger than today's Pacific, and the Indian Ocean had a more complex geometry.

Two important paleogeographic changes took place during the early Cenozoic: the opening and closing of oceanic gateways between the continents and the uplift of the Himalayas and Tibetan Plateau. Probably the single most important paleoclimatic event during the Cenozoic was the formation of the north and south polar ice caps. The Antarctic ice cap started to grow in the late Eocene (~40 Ma) as a result of the geographic isolation of Antarctica. The Arctic ice cap is much younger, and a permanent ice cap did not appear until the Pliocene (~5 Ma).

The isolation of Antarctica resulted from the opening of two oceanic gateways: the Tasman Straits and the Drake Passage (Lawver & Gahagan 2003). When the Southeast Indian Ocean between southern Australia and Antarctica (Wilkes Land) began to open in the Late Cretaceous, the rifted margin made a right-angle bend, hooking around Tasmania. This strike-slip boundary, the Tasman Fracture Zone, effectively closed off the eastern end of the Southeast Indian Ocean during the earliest phases of opening. Australia began to move rapidly northward during the late Eocene (40–35 Ma), and the overlapping bits of the Australian and Antarctic Plates (South Tasman Rise and North Victoria Land, respectively) separated, allowing deep waters from the Indian Ocean and South Pacific Ocean to mix. The first deep-water connection between the Indian Ocean and the South Pacific was through the Tasman Straits.

The opening of the Drake Passage between the southern tip of South America (Patagonia) and the northern tip of the West Antarctic Peninsula (Palmer Peninsula) followed shortly. In the early Mesozoic these two regions were part of a continuous Andean mountain range. The ligation between Patagonia and the Palmer Peninsula was tested when Gondwana began to rift apart in the Late Jurassic. Despite being stretched and extended as the Weddell Sea opened during the Cretaceous, Patagonia and the Palmer Peninsula were not completely separate until the late Eocene (~40 Ma). This opening happened in two phases: The shallow-water connection (<1,000 m) was established by 45 Ma, and the deep-water connection (>1,000 m) took place ~10 million years later (Livermore et al. 2005). An age of 41 Ma for the opening of the Drake Passage is based on the change in neodymium isotope ratios from sediments on the Agulhas Ridge that suggests an influx of shallow Pacific water (Scher & Martin 2006).

The rapid 4°C drop in global temperature across the Eocene–Oligocene boundary (**Figure 19**) followed the growth of the south polar ice cap and the complete isolation of Antarctica from the world's oceans. This event marked the beginning of the Cenozoic Icehouse. The seeds of global cooling were planted millions of years earlier, during the height of the Paleocene–Eocene Hothouse. As illustrated in **Figure 19**, the Cenozoic cooling trend began after the Early Eocene Thermal Maximum (EETM) (52–50 Ma) and continued during the middle and late Eocene. The generally accepted explanation is that the collision of India with south-central Asia, which took place at the height of the EETM [~50 Ma (Molnar & Tapponnier 1975; Rowley 1996, 1998)], triggered a cascade of events that led to global cooling (Raymo & Ruddiman 1992). This massive collision resulted in the rapid uplift of the Himalayas Mountains followed by the rise of the Tibetan Plateau. These young mountains were in the path of the Asian monsoon, which brought warm temperatures and abundant moisture. This led to rapid mechanical and chemical weathering. The flux of calcium cations to the world's oceans drew down the amount of CO₂ in the atmosphere. The gradual decrease in atmospheric CO₂ cooled Earth.

As noted earlier, the Drake Passage and the Tasman oceanic gateway had profound effects on oceanic circulation and global climate during the early and middle Cenozoic. Four other late Cenozoic oceanic gateways are worth mentioning: the Panama land bridge, the Sunda Seaway, the Neotethys Seaway (Paratethys), and the Straits of Gibraltar.

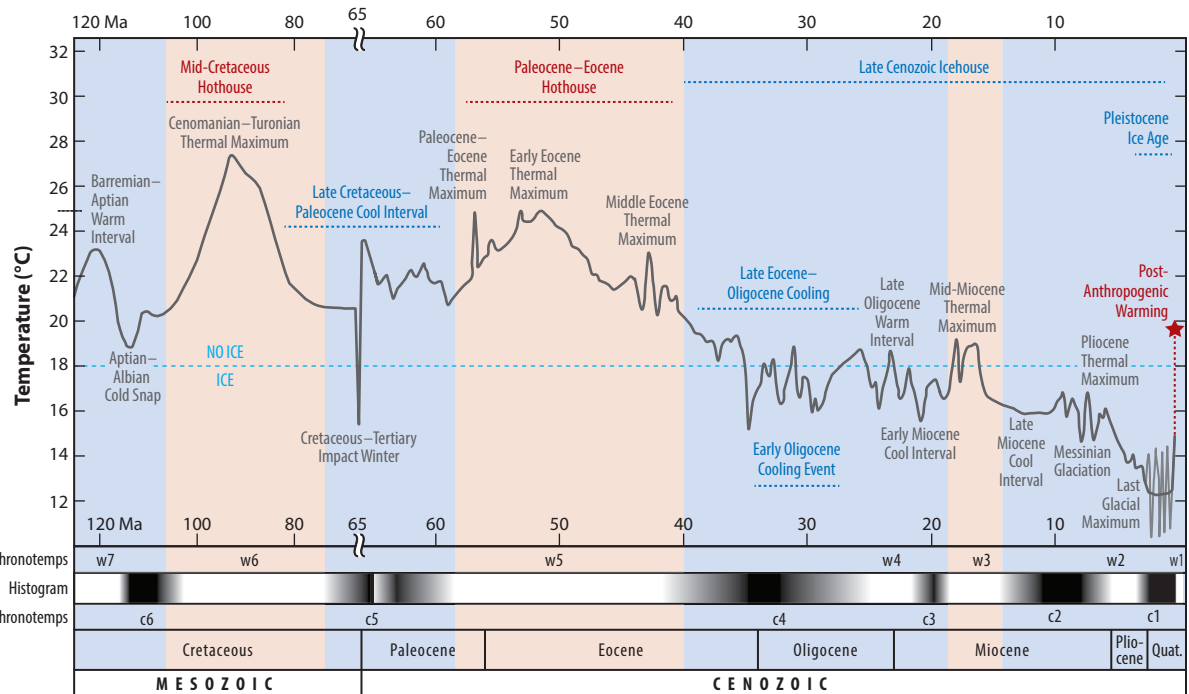


Figure 19

A Cenozoic paleotemperature timescale. Warm time intervals are white; cool time intervals are black. The light gray jagged lines are a schematic representation of more than 50 glacial/interglacial cycles during the Plio–Pleistocene. The solid gray line is the Global Average Temperature. Large permanent ice caps are at less than 18°C; no large permanent ice caps are at greater than 18°C. The timescale is from the International Chronostratigraphic Chart version 2020/01. Refer to Table 3 for more information about each chronotemp. Figure adapted from Scotese et al. (2021).

The Panama land bridge is built on volcanic island arcs that date back to the mid-Cretaceous (100–84 Ma) (Pindell & Kennan 2009). First appearing as isolated islands (Late Cretaceous) and then coalescing into island clusters (Paleocene), a throughgoing submarine ridge had appeared by the Eocene (**Figure 9**). Free migration of terrestrial faunas between North and South America during the Eocene was not possible and could be achieved only by island hopping. By the early Oligocene much of the submarine portion of Panama was fully constructed, and although shallow marine waters continued to flow between the oceans, the isthmus prevented the interchange of deep waters between the Atlantic and Pacific Oceans. In the late Neogene (4–5 Ma), the Panama volcanic archipelago rose above sea level, creating the Panama land bridge. This land bridge connected North and South America, permitting the interchange of fauna and flora (Marshall et al. 1982). More importantly, this land bridge served as a complete blockade, isolating the equatorial Atlantic and Pacific Oceans. Warm, equatorial Atlantic waters were diverted northward (the Gulf Stream). The warm waters of the Gulf Stream warmed the Arctic regions and provided a new source of moisture, which fed winter snows. Increased snowfall led to the growth of glaciers, and the Arctic ice sheets grew large (Herman & Hopkins 1980).

In the Eastern Hemisphere, the northward movement of Australia during the early Miocene and the collision of New Guinea with Southeast Asia during the middle–late Miocene (~10–15 Ma) blocked equatorial circulation between the western Pacific Ocean and the Indian Ocean (Sunda Seaway). As a consequence, the distance that ocean waters circulated along the Equator was

shortened, resulting in a net cooling of tropical surface waters. This reduction in Earth's thermal budget, in turn, may have led to increased cooling at the poles.

Paratethys is the name given to the last remnants of the Neotethys Seaway in Europe and the Mideast (Steininger & Wessley 2000) (**Figure 18**). By the early Oligocene, the collision between the Arabian Peninsula and Iran was nearly complete. Although all the ocean floor had been subducted, a shallow seaway, the proto-Persian Gulf, filled the foredeep of the Zagros Mountains of Iran and Iraq. During brief highstands of sea level during the late Oligocene and early Miocene, this shallow seaway connected with the deeper waters of the eastern Mediterranean. The closure of this westernmost extension of the Tethys in the earliest Oligocene eliminated the westward flowing Subtropical Eocene Neotethys current. Some authors have speculated that this may have contributed to global cooling during the early Oligocene (Hotinski & Toggweiler 2003, Jovane et al. 2009, Toggweiler & Björnsson 2000).

Finally, a noteworthy paleogeographic change that had paleoclimatic implications occurred at the very end of the Miocene. During the Messinian stage (~6 Ma), both the eastern and western ends (Straits of Gibraltar) of the Mediterranean were closed off. The isolation of the Mediterranean from the world's oceans was due to an uplift caused by Africa's northward convergence with Southern Europe and a fall in sea level due to the growth of the Antarctic ice cap. This isolation resulted in the evaporation and desiccation of most of the Mediterranean Basin [Messinian event (Hsü et al. 1977)]. Thick salt deposits were formed throughout the Mediterranean during this event. It should be noted that the desiccation of the Mediterranean Basin took place because the Mediterranean Basin was located in the dry northern subtropics. If the Mediterranean had been located along the Equator, in the equatorial rainy belt, a large inland freshwater sea would have formed.

5. SUMMARY AND CONCLUSIONS

There are three great phases of Phanerozoic paleogeography. During the early phase (540–360 Ma), a large supercontinent (Gondwana) occupied most of the Southern Hemisphere and several medium-sized continents (Laurentia, Baltica, and Siberia) straddled the Equator. During the middle phase (360–180 Ma), the continents were joined together in a Pangean supercontinent that stretched from the South Pole to the North Pole. During this phase, an even larger superocean, Panthalassa, occupied the opposite hemisphere. During the final phase (180 Ma to modern times), Pangea broke apart into six large continents separated by expanding oceans. We may now be entering a phase that will see the closure of these intra-Pangean oceans and the formation of a new supercontinent, Pangea Proxima, at some distant time in the future (~250 million years; Overbye 1982; see also **Supplemental Appendix 3**).

These three phases of paleogeographic change were driven by three important paleogeographic trends. The first trend is the inexorable transfer of continental material from the Southern Hemisphere to the Northern Hemisphere. As illustrated in **Figure 16**, during the first 150 million years of the Phanerozoic, the percentage of land area in the Northern Hemisphere was negligible (~10%). The percentage of land in the Northern Hemisphere grew steadily during the next 400 million years. Some localities (e.g., Greenland, Scotland, and Northern Ireland) have not only crossed from the Southern Hemisphere into the Northern Hemisphere but also moved from a south polar location to a position near the North Pole (**Figure 20**; see sidebar titled The Polar Express). It is likely that the northward migration of continents will continue for tens of millions of years into the future due to the continued northward convergence of Africa and Australia and, to a lesser extent, India and South America.

The second major trend, the emergence of the continents and the increase in global land area, is illustrated in **Figure 21**. At the beginning of the Cambrian, the proportion of continental

Supplemental Material >

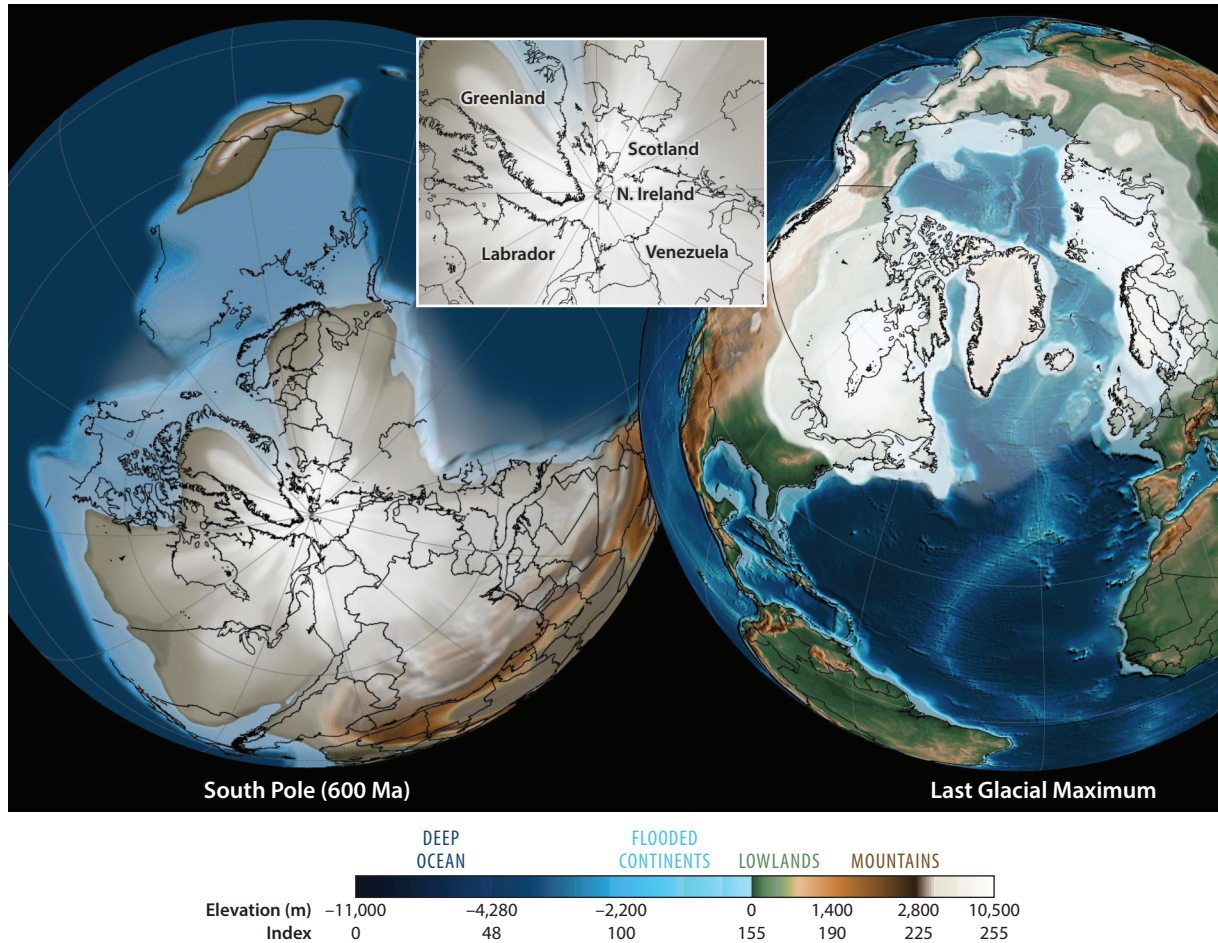


Figure 20

Maps illustrating the location of Greenland, Northern Ireland, and Scotland during the late Precambrian (600 Ma; South Pole) and the Last Glacial Maximum (20,000 years ago).

material that was land was approximately equal to the proportion of continent that was flooded by broad inland seas—also known as epeiric seas. The amount of continental flooding increased during the Ordovician and remained high during the Silurian and Devonian—with the exception of the great Hirnantian Ice Age (444 Ma) when an extensive south polar ice cap withdrew water from the oceans and sea level fell more than 200 m (Rasmussen et al. 2019). Starting in the Late Devonian, the relative amount of land began to increase dramatically. During the Carboniferous, Permian, and Triassic and into the Early Jurassic, the global area of dry land nearly doubled (17% to 31%). This trend was reversed in the Middle Jurassic when Pangea began to break apart. Notable sea level highstands occurred during the Late Jurassic (160 Ma), Early Cretaceous (120 Ma), and middle Cretaceous (90 Ma). Immediately following the Cenomanian–Turonian highstand (93 Ma) and continuing into the Cenozoic, the proportion of land began to rapidly increase as the supercontinent of Eurasia was assembled. The increasing frequency and magnitude of continental collisions (Alpine, Turkey-Caucasus, and Himalayan-Tibetan) combined with the growth of the Antarctic and Greenland ice caps have left the modern continents high and dry.

THE POLAR EXPRESS

As **Figure 16** illustrates, there has been a steady movement of continents northward since the Middle Devonian (~380 Ma). In these figures, the northward movement of the continents is represented by the increasing continental area above the Equator. In the Early Devonian, ~90% of the continents were located south of the Equator. In the modern world, 68% of the continents occupy the Northern Hemisphere. The northward journey of India is well known. When India rifted away from Madagascar 90 million years ago, it was located 35° south of the Equator; it is now located 20° north of the Equator. It traversed the intervening 6,000 km at rates up to 20 cm/year. However, India does not hold the record for northward migration. As shown in **Figure 20**, 600 million years ago, the continental terranes that make up modern Scotland, Northern Ireland, and southern Greenland were located very close to the South Pole (inset map, **Figure 20**). During the past 600 million years, Scotland, Northern Ireland, and southern Greenland have migrated ~145° northward—a journey of more than 16,000 km.

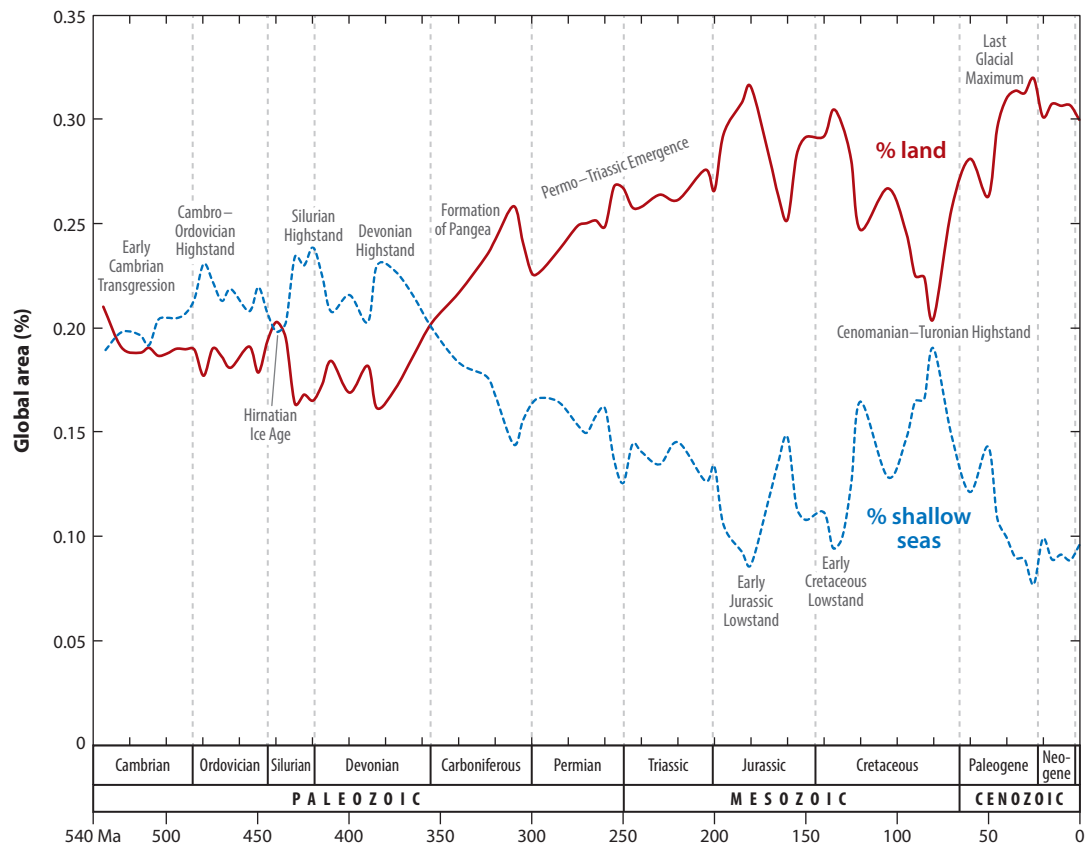


Figure 21

Land area and continental flooding during the Phanerozoic. Figure adapted from Kocsis & Scotese (2020).

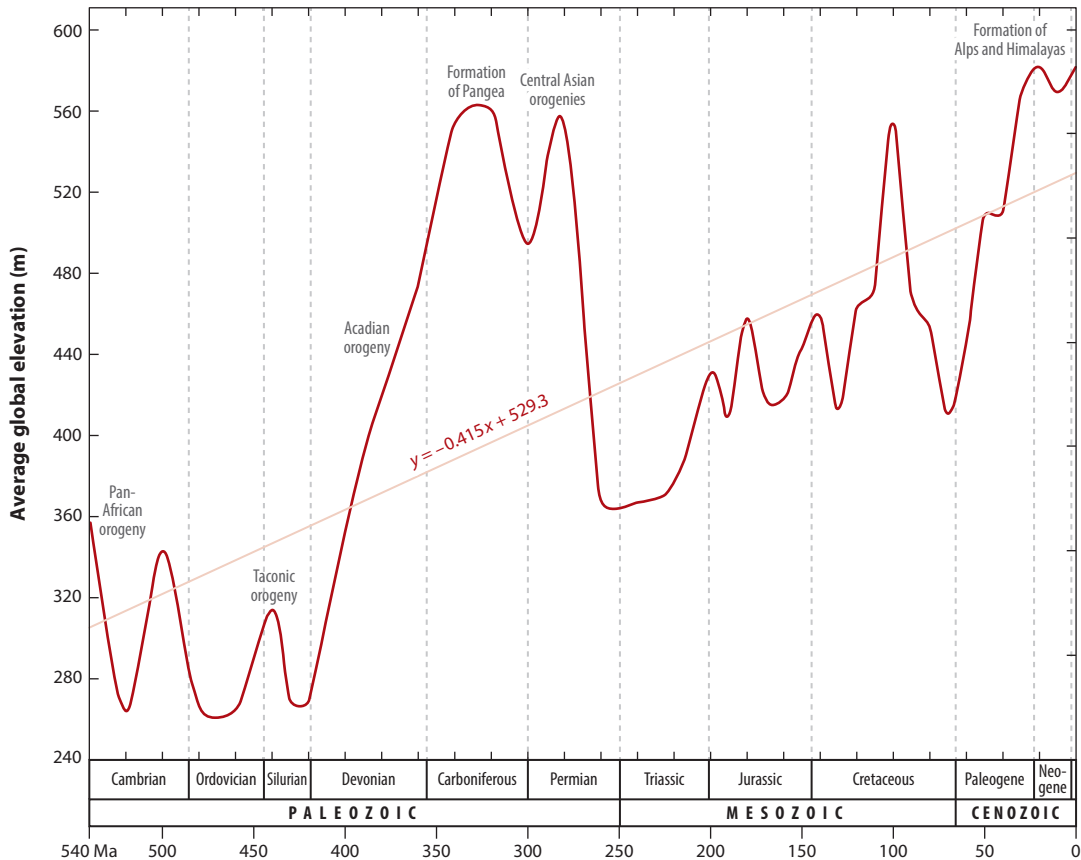


Figure 22

Average elevation of land during the Phanerozoic. Figure adapted from Kocsis & Scotese (2020).

The third major paleogeographic trend is more subtle. Since the Late Ordovician (~ 440 Ma) there has been a steady increase in average elevation of the continents (Figure 22). This trend is certainly related to the emergence of the continents. As a consequence of the long history of continent-continent collisions, the average elevation of the continents has increased from ~ 300 m in the early Paleozoic to nearly 600 m today. This translates into an approximately half-meter increase per 1 million years in the average height of the land. This increase in elevation has not been constant but rather has occurred in pulses of mountain building due to the series of continent-continent collisions that formed Pangea, Eurasia, and, to a lesser extent, North America. It should be noted that the measure of elevation used in this estimate is the height of the continents obtained from the digital models of elevation used to produce the paleogeographic reconstructions (Scotese & Wright 2018).

Because the mean radius of Earth has not changed through time [i.e., no Earth expansion (Rowley 2017)], the increase in the average elevation of the continents must be accompanied by a corresponding increase in the average depth of the oceans. Any continental uplift must be balanced by an equal amount of oceanic subsidence. Sea level has been falling, in general, throughout the Phanerozoic for two reasons: Continents have become more emergent, and the volume of the ocean basins has been increasing. Larger ocean basins provide more room for

the ocean's water. We assume that the volume of ocean water has not increased or decreased significantly during the past 540 million years. A corollary of this observation is that the ocean basins must have been shallower during the early and middle Paleozoic, which implies faster seafloor spreading rates or more mid-ocean ridges.

6. CLOSING THOUGHTS

I have often pondered what Amadeus Grabau meant when he said on the last page of his two-volume treatise on Earth history that he hoped that paleogeography would eventually become “the crowning attraction to the student of Earth history.” The study of Earth sciences is filled with innumerable fascinating stories that need to be told, including the elucidation of processes taking place deep within Earth; understanding the complex linkages between solid earth, the oceans, the atmosphere, and the biosphere; and retelling the story of how global environmental changes have guided the evolution of life on Earth. Why should paleogeography be so special? Upon reflection, I think Grabau was trying to tell us that paleogeography requires the integration of nearly every aspect of Earth sciences in order to build a global picture of what Earth was like and how it has changed through time. When done well, paleogeography constructs the geological virtual reality that every geologist hopes to inhabit. Paleogeography is a mental time machine that allows us to travel back to any ancient world and imagine the processes that were taking place and how they transformed the ancient Earth into the modern world.

Our present attempts to imagine past worlds are rudimentary at best. We are standing on the shoulders of the last generation of paleogeographers—such as Dercourt, Cook, Khain, Ronov, Vinogradov, Wang, Ziegler, and Zonenshain—who in turn stood on the shoulders of the first generation of paleogeographers such as Grabau and Schuchert. Each generation of paleogeographers is able to peer a little bit further back into the past and unravel a little more of the story of Earth history. It will be up to the next generation of paleogeographers to assemble the data and information that have been collected during the past 300 years of geological mapping and exploration, to combine them with constantly improving technology and big data analysis tools, to reveal the hidden details of Earth history, and to build the ultimate Earth system time machine.

I conclude with the lyrics from a song I wrote many years ago:

Sailing along on uncharted seas, who knows what we might find.
You needn't go far to take this trip because the journey's through your mind.
The key to the future lies locked in the past.
There's always a question that hasn't been asked.
So come along and sail with me, who knows what we might find.
You needn't go far to take this trip because the journey's through your mind!

—*The Paleogeographer's Song* (Martin & Petrova 2011)

DISCLOSURE STATEMENT

The author is not aware of any affiliations, memberships, funding, or financial holdings that might be perceived as affecting the objectivity of this review.

ACKNOWLEDGMENTS

C.R.S. thanks Adam Kocsis and Wolfgang Kiessling for their thoughtful reviews and constructive suggestions. He received support to produce the maps in the Paleogeographical Atlas from the PALEOMAP Project industrial consortium (2003–2013) and thanks innumerable friends,

mentors, and enthusiastic supporters through the years, in particular A.M. Ziegler, W.S. McKerrow, R. van der Voo, S. Snelson, J. Westrich, and A.J. Boucot. He extends special thanks to Phyllis Richmond for correcting grammar, clarifying prose, and corralling verbiage.

LITERATURE CITED

- Algeo TJ, Seslavinsky KB. 1995. Reconstructing eustasy and epeirogenic trends from Paleozoic continental flooding records. In *Sequence Stratigraphy and Depositional Response to Eustatic, Tectonic and Climate Forcing*, ed. BU Haq, pp. 209–46. Dordrecht, Neth.: Kluwer
- Alroy J, Aberhan M, Bottjer DJ, Foote M, Fürsich FT, et al. 2008. Phanerozoic trends in the global diversity of marine invertebrates. *Science* 321:97–100
- Baatsen M, van Hinsbergen DJJ, von der Heydt AS, Dijkstra HA, Sluijs A, et al. 2015. A generalized approach for reconstructing geographical boundary conditions for palaeoclimate modeling. *Clim. Past Discuss.* 11:4917–42
- Barrier E, Vrielynck B. 2008. *Palaeotectonic Maps of the Middle East, Middle East Basins and Evolution Programme, Atlas of 14 maps, Tectono-Sedimentary-Palinspastic maps from the Late Norian to the Pliocene*. Maps, Commiss. Geolog. Map World, Paris
- Blakey RC. 2002. *Global Paleogeography, Rectilinear Projection (DVD)*. Flagstaff, AZ: Colo. Plateau Geosyst.
- Blakey RC. 2008. Gondwana paleogeography from assembly to breakup—a 500 m.y. odyssey. *Geol. Soc. Am. Spec. Pap.* 441:1–28
- Blakey RC, Ranney WD. 2018. *Ancient Landscapes of Western North America*. Cham, Switz.: Springer
- Boucot AJ. 1975. *Evolution and Extinction Rate Controls: Developments in Palaeontology and Stratigraphy*. Amsterdam: Elsevier
- Boucot AJ, Gray J. 1976. Epilogue: a Paleozoic Pangea? In *Historical Biogeography, Plate Tectonics, and the Changing Environment*, ed J Gray, AJ Boucot, pp. 465–82. Corvallis, OR: Or. State Univ. Press
- Boucot AJ, Xu C, Scotese CR, Morley RJ. 2013. *Phanerozoic Paleoclimate: An Atlas of Lithologic Indicators of Climate*. Tulsa, OK: SEPM
- Bozhko NA, Khain VE. 1987. *Gondwana Paleotectonic Maps*. Maps, Geolog. Complex Cent. Reg. USSR
- Brenchley PJ, Marshall JD, Carden GAF, Robertson DBR, Long DG, et al. 1994. Bathymetric and isotopic evidence for a short-lived Late Ordovician glaciation in a greenhouse period. *Geology* 22:295–98
- Brownstein CD. 2018. The biology and ecology of non-avian dinosaurs of Appalachia. *Palaeontol. Electron.* 21:1–56
- Caputo MV, de Melo JHG, Strel M, Isbell JL. 2008. Late Devonian and Early Carboniferous glacial records of South America. *Geol. Soc. Am. Spec. Pap.* 441:161–74
- Chumakov NM. 1994. Evidence of Late Permian glaciation in the Kolyma River Basin: a repercussion of the Gondwana glaciations in northeast Asia? *Stratigr. Geol. Correl.* 2(5):426–44
- Chumakov NM, Zharkov MA. 2003. Climate during the Permian–Triassic biosphere reorganizations. Article 2. Climate of the Late Permian and Early Triassic: general inferences. *Stratigr. Geol. Correl.* 11(4):361–75
- Colbert EH. 1982. The distribution of Lystrosaurus in Pangea and its implications. *Geobios* 15:375–83
- Cook PJ. 1990. *Australia: Evolution of a Continent*. Canberra, Aust.: Aust. Gov. Publ. Serv.
- Cook TD, Bally AW. 1975. *Stratigraphic Atlas of North America and Central America*. Princeton, NJ: Princeton Univ. Press
- Cope JCW, Ingham JK, Rawson F. 1992. *Atlas of Paleogeography and Lithofacies*. London: Geol. Soc.
- Copper P. 2002. Silurian and Devonian reefs: 80 million years of global greenhouse between two ice ages. *SEPM Spec. Publ.* 72:181–238
- Copper P, Scotese CR. 2003. Megareefs in Middle Devonian supergreenhouse climates. *Geol. Soc. Am. Spec. Pap.* 370:209–30
- Crowley TJ. 1994. Pangean climates. *Geol. Soc. Am. Spec. Pap.* 288:25–39
- Crowley TJ, Baum SK. 1991. Toward reconciliation of Late Ordovician (~440 Ma) glaciation with very high CO₂ levels. *J. Geophys. Res.* 96(D12):22597–610
- Dalziel IWD. 1991. Pacific margins of Laurentia and East Antarctica as a conjugate rift pair: evidence and implications for an Eocambrian supercontinent. *Geology* 19:598–601

- Demaison GJ, Moore GT. 1980. Anoxic environments and oil source bed genesis. *AAPG Bull.* 64:1179–209
- Dercourt J, Gaettani M, Vrielynck B, Barrier E, Biju-Duval B, et al. 2000. *Atlas Peri-Tethys: Palaeogeographical Maps*. Paris: Comm. Geol. Map World
- Dercourt J, Ricou LE, Vrielynck B. 1993. *Atlas Tethys: Palaeoenvironmental Maps*. Paris: Gauthier-Villars
- Dercourt J, Zonenshain L, Ricou L, Kazmin VG, Le Pichon X, et al. 1985. Presentation de 9 cartes paleogeographiques au 1/20.000.000 s'étendant de l'Atlantique au Pamir pour la période du Lias à l'Actuel. *Bull. Soc. Geo. Fr.* 8(5):637–52
- DiMichele WA, Montañez IP, Poulsen CJ, Tabor NJ. 2009. Climate and vegetational regime shifts in the late Paleozoic ice age Earth. *Geobiology* 7:200–26
- Domeier M. 2016. A plate tectonic scenario for the Iapetus and Rheic oceans. *Gondwana Res.* 36:275–95
- Domeier M. 2018. Early Paleozoic tectonics of Asia: towards a full-plate model. *Geosci. Front.* 9:789–862
- Domeier M, Torsvik TH. 2014. Plate tectonics in the late Paleozoic. *Geosci. Front.* 5:303–50
- Domeier M, Torsvik TH. 2017. Full-plate modelling in pre-Jurassic time. *Geol. Mag.* 156(2):261–80
- Erba E, Duncan RA, Bottini C, Tiraboschi D, Weissert H, et al. 2015. Environmental consequences of Ontong Java Plateau and Kerguelen Plateau volcanism. *Geol. Soc. Am. Spec. Pap.* 511:271–303
- Ernst RE. 2014. *Large Igneous Provinces*. Cambridge, UK: Cambridge Univ. Press
- Evans D, Graham C, Armour A, Bathurst P. 2003. *The Millennium Atlas: Petroleum Geology of the Central and Northern North Sea*. London: Geol. Soc.
- Fensome RA, Williams GL. 2001. *The Last Billion Years: The Geological History of the Maritime Provinces of Canada*. Halifax, Can.: Nimbus
- Finnegan S, Bergmann K, Eiler JM, Jones DS, Fike DA, et al. 2011. The magnitude and duration of Late Ordovician-Early Silurian glaciation. *Science* 331(6019):903–6
- Godderis Y, Donnadieu Y, Carretier S, Aretz M, Dera G, et al. 2017. Onset and ending of the late Palaeozoic ice age triggered by tectonically paced rock weathering. *Nat. Geosci.* 10(5):382–85
- Godderis Y, Donnadieu Y, Le Hir G, LeFebvre V, Nardin E. 2014. The role of palaeogeography in the Phanerozoic history of atmospheric CO₂ and climate. *Earth-Sci. Rev.* 128:122–38
- Golonka J. 2000. *Cambrian-Neogene Plate Tectonic Maps*. Krakow, Pol.: Druk. Univ. Jagiell.
- Golonka J. 2007. Late Triassic and Early Jurassic paleogeography of the world. *Palaeogeogr. Palaeoclimatol. Palaeoecol.* 244:297–307
- Grabau A. 1924. *Principles of Stratigraphy*, Vol. 1 & 2. New York: Dover
- Hallam A. 1984. Pre-Quaternary sea-level changes. *Annu. Rev. Earth Planet. Sci.* 12:205–43
- Haq BU, Hardenbol J, Vail PR. 1987. Chronology of fluctuating sea levels since the Triassic. *Science* 235:1156–67
- Haq BU, Schutter SR. 2009. A chronology of Paleozoic sea-level changes. *Science* 322:64–68
- Hay WW. 2017. Toward understanding Cretaceous climate—an updated review. *Sci. China Earth Sci.* 60:5–19
- Haywood AM, Valdes PJ, Aze T, Barlow NA, Dolan AM, et al. 2019. What can palaeoclimate modelling do for you? *Earth Syst. Environ.* 3(1):1–18
- Herman Y, Hopkins DM. 1980. Arctic oceanic climate in late Cenozoic times. *Science* 209(4456):557–62
- Herrle JO, Schröder-Adams CJ, Davis W, Pugh AT, Galloway JM, Fath J. 2015. Mid-Cretaceous High Arctic stratigraphy, climate, and oceanic anoxic events. *Geology* 43(5):403–6
- Hoffman PF. 1991. Did the breakout of Laurentia turn Gondwanaland inside out? *Science* 252:1409–12
- Hoffman PF, Kaufman AJ, Halverson GP, Schrag DP. 1998. A Neoproterozoic snowball Earth. *Science* 281:1342–46
- Hotinski RM, Toggweiler JR. 2003. Impact of a Tethyan circumglobal passage on ocean heat transport and “equable” climates. *Paleoceanography* 18:1007–15
- Hsü KJ, Montadert L, Bernoulli D, Cita MB, Erickson A, et al. 1977. History of the Mediterranean salinity crisis. *Nature* 267:399–403
- Isozaki Y. 1997. Permo-Triassic boundary superanoxia and stratified superocean: records from lost deep sea. *Science* 276:235–38
- Jakobsson M, MacNab R, Cherkis N, Schenke H-W. 2004. *The International Bathymetric Chart of the Arctic Ocean (IBCAO)*. Boulder, CO: Natl. Geophys. Data Cent.
- Johnson JG. 1974. Extinction of perched faunas. *Geology* 2:479–82

- Joshi MM, Mills BJW, Johnson M. 2019. A capacitor-discharge mechanism to explain the timing of orogeny-related global glaciations. *Geophys. Res. Lett.* 46:8347–54
- Jovane L, Coccioni R, Marsili A, Acton G. 2009. The late Eocene greenhouse–icehouse transition: observations from the Massignano global stratotype and point (GSSP). *Geol. Soc. Am. Spec. Pap.* 452:149–68
- Kazmin VG, Natapov LM. 1998. *The Paleogeographic Atlas of Northern Eurasia: Paleogeographic Maps on the Palinspastic Reconstruction (Orthographic Projection)*. Moscow: Russ. Acad. Nat. Sci.
- Keller B, Husson JM, Mitchell RN, Bottke WF, Gernon TM, et al. 2019. Neoproterozoic glacial origin of the Great Unconformity. *PNAS* 116(4):1136–45
- Kiessling W, Flügel E, Golonka J. 2002. *Phanerozoic Reef Patterns*. Tulsa, OK: SEPM
- Kocsis AT, Scotese CR. 2020. Mapping paleocoastlines and continental flooding during the Phanerozoic. *Earth-Sci. Rev.* 213:103463
- Kump LR, Arthur MA. 1999. Interpreting carbon-isotope excursions: carbonates and organic matter. *Chem. Geol.* 161:181–98
- Kump LR, Gibbs MT, Arthur MA, Patzkowsky ME, Sheehan PM. 1995. Hirnantian glaciation and the carbon cycle. In *Ordovician Odyssey: Short Papers for the Seventh International Symposium on the Ordovician System, Las Vegas, Nevada, USA, June, 1995*, ed. JD Cooper, ML Droser, SC Finney, pp. 299–302. Fullerton, CA: SEPM
- Kump LR, Kasting JF, Crane RG. 1999. *The Earth System*. Upper Saddle River, NJ: Prentice Hall
- Lawver LA, Gahagan LM. 2003. Evolution of Cenozoic seaways in the circum-Antarctic region. *Paleogeogr. Palaeoclimatol. Palaeoecol.* 198:11–37
- Lawver LA, Scotese CR. 1987. A revised reconstruction of Gondwanaland. In *Gondwana Six: Structure, Tectonics and Geophysics*, ed. GD McKenzie, pp. 17–24. Washington, DC: Am. Geophys. Union
- Lenton TM, Crouch M, Johnson M, Pires N, Dolan L. 2012. First plants cooled the Ordovician. *Nat. Geosci.* 5:86–89
- Ling M-X, Zhan R-B, Wang G-X, Wang Y, Amelin Y, et al. 2019. An extremely brief end Ordovician mass extinction linked to abrupt onset of glaciation. *Solid Earth Sci.* 4(4):190–98
- Livermore R, Nankivell A, Eagles G, Morris P. 2005. Paleogene opening of the Drake Passage. *Earth Planet. Sci. Lett.* 236:459–70
- Lythe MB, Vaughan DG, BEDMAP Consort. 2000. *BEDMAP: Bed Topography of the Antarctic*, Misc. 9, scale 1:10,000,000. Cambridge, UK: Br. Antarct. Surv.
- Ma YS, Chen HD, Wang GL. 2009. *Atlas of Tectonics: Sequence Lithofacies Paleogeography in South China*. Beijing: Science Press
- Mallory WW. 1972. *Geological Atlas of the Rocky Mountain Region*. Denver, CO: Rocky Mt. Assoc. Geol.
- Markwick PJ. 2019. Palaeogeography in exploration. *Geol. Mag.* 156(2):366–407
- Marshall LG, Webb DS, Sepkoski JJ, Raup DM. 1982. Mammalian evolution and the great American interchange. *Science* 215:1351–57
- Martin A, Petrova L. 2011. *The Paleogeographer’s Song*. Denton: Univ. N. Texas Dep. Radio Telev. Film. <https://www.youtube.com/watch?v=7qesJYbwKtY>
- Matthews KJ, Maloney KT, Zahirovic S, Williams S, Seton M, Müller RD. 2016. Global plate boundary evolution and kinematics since the late Paleozoic. *Glob. Planet. Change* 146:226–50
- McCrossan RG, Glaister RP, Austin GH, Nelson SJ. 1964. *Geological History of Western Canada*. Calgary, Can.: Alberta Soc. Pet. Geol.
- McKenna MC. 1973. Sweepstakes, filters, corridors, Noah’s arks, and beached Viking funeral ships and palaeogeography. In *Implications of Continental Drift to the Earth Sciences*, ed. DH Tarling, SK Runcorn, pp. 293–308. New York: Academic
- Meert JG. 2003. A synopsis of events related to the assembly of eastern Gondwana. *Tectonophysics* 362:1–40
- Meingold G, Sengör AMC. 2019. An historical account of how continental drift and plate tectonics provided the framework for our current understanding of palaeogeography. *Geol. Mag.* 156(2):182–207
- Miller KG, Kominz MA, Browning JV, Wright JD, Mountain GS, et al. 2005. The Phanerozoic record of global sea-level change. *Science* 310:1293–98
- Molnar P, Tapponier P. 1975. Cenozoic tectonics of Asia: effects of a continental collision. *Science* 189:419–26
- Montañez IP, McElwain JC, Poulsen CJ, White JD, Dimichele WA, et al. 2016. Climate, $p\text{CO}_2$ and terrestrial carbon cycle linkages during late Palaeozoic glacial–interglacial cycles. *Nat. Geosci.* 9:824–28

- Montañez IP, Poulsen JC. 2013. The Late Paleozoic ice age: an evolving paradigm. *Annu. Rev. Earth Planet. Sci.* 41:629–56
- Montañez IP, Tabor NJ, Niemeier D, DiMichele WA, Frank TD, et al. 2007. CO₂-forced climate and vegetation instability during Late Paleozoic deglaciation. *Science* 315:87–91
- Moore TL, Scotese CR. 2010. The Paleoclimate Atlas (ArcGIS). *Geol. Soc. Am. Abstr. Programs* 42:598
- Moores EM. 1991. Southwest U.S.–East Antarctica (SWEAT) connection: a hypothesis. *Geology* 19:425–28
- Müller RD, Cannon J, Qin X, Watson RJ, Gurnis M, et al. 2018. GPlates: building a virtual Earth through deep time. *Geochem. Geophys. Geosyst.* 19:2243–61
- Müller RD, Dutkiewicz A, Seton M, Gaina C. 2013. Seawater chemistry driven by supercontinent assembly, breakup, and dispersal. *Geology* 41(8):907–10
- Müller RD, Roest WR, Royer JY, Gahagan LM, Sclater JG. 1993. *A Digital Age Map of the Ocean Floor*. La Jolla, CA: Scripps Inst. Oceanogr.
- Müller RD, Roest WR, Royer JY, Gahagan LM, Sclater JG. 1997. Digital isochrons of the world's ocean floor. *J. Geophys. Res.* 102(B2):3211–14
- Müller RD, Sdrolias M, Gaina C, Roest WR. 2008a. Age, spreading rates, and spreading asymmetry of the world's ocean crust. *Geochem. Geophys. Geosyst.* 9(4):Q04006
- Müller RD, Sdrolias M, Gaina C, Steinberger B, Heine C. 2008b. Long-term sea-level fluctuations driven by ocean basin dynamics. *Science* 319:1357–62
- Müller RD, Seton M, Zahirovic S, Williams SE, Matthews K, et al. 2016. Ocean basin evolution and global-scale plate reorganization events since Pangea breakup. *Annu. Rev. Earth Planet. Sci.* 44:107–38
- Murphy JB, Strachan RA, Quesada C. 2021. Pannotia to Pangaea: Neoproterozoic and Paleozoic Orogenic cycles in the Circum-Atlantic region: a celebration of the career of Damian Nance. *Geol. Soc. Lond. Spec. Publ.* 503:1–11
- Osen AK, Winguth AME, Winguth C, Scotese CR. 2013. Sensitivity of Late Permian climate to bathymetric features and implications for the mass extinction. *Glob. Planet. Change* 105:171–79
- Overbye D. 1982. The shape of tomorrow: an imaginative Chicago geologist plots the wanderings of the continents to try to read the shape of the future. *Discover* 3(11):20–25
- Parrish JT. 1993. Climate of the supercontinent Pangea. *J. Geol.* 101:217–35
- Parsons B, Sclater JG. 1977. An analysis of the variation of ocean floor bathymetry and heat flow with age. *J. Geophys. Res.* 82(5):803–27
- Peltier WR. 2004. Global glacial isostasy and the surface of the ice-age Earth: the ICE-5G (VM2) model and GRACE. *Annu. Rev. Earth Planet. Sci.* 32:111–49
- Pindell J, Kennan L. 2009. Tectonic evolution of the Gulf of Mexico, Caribbean, and northern South America in the mantle reference frame: an update. *Geol. Soc. Lond. Spec. Publ.* 328:1–55
- Powell CM, Young GM. 1995. Are Neoproterozoic glacial deposits preserved on the margins of Laurentia related to the fragmentation of two supercontinents? *Geology* 23:1053–55
- Rasmussen CMO, Kroger B, Nielsen ML, Colmenar J. 2019. Cascading trend of early Paleozoic marine radiations paused by late Ordovician extinctions. *PNAS* 116(15):7207–13
- Raymo ME, Ruddiman WF. 1992. Tectonic forcing of late Cenozoic climate. *Nature* 359:117–22
- Rees M, Ziegler AM, Gibbs MT, Kutzbach JE, Behling PJ, Rowley DB. 2002. Permian phytogeographic patterns and climate data/model comparisons. *J. Geol.* 110:1–31
- Rees M, Ziegler AM, Valdes J. 2000. Jurassic phytogeography and climates: new data and model comparisons. In *Warm Climates in Earth History*, ed. BT Huber, KG Macleod, SL Wing, pp. 297–318. Cambridge, UK: Cambridge Univ. Press
- Richey JD, Montañez IP, Godderis Y, Looy CV, Griffis NP, DiMichele WA. 2020. Influence of temporally varying weatherability on CO₂–climate coupling and ecosystem change in the late Paleozoic. *Clim. Past* 16(5):1759–75
- Rong JY. 1984. Distribution of the *Hirnantia* fauna and its meaning. In *Aspects of the Ordovician System*, ed. DL Bruton, pp. 101–12. Oslo, Nor.: Universitetsforlaget
- Ronov AB, Khain YE, Balukhovsky A. 1989. *Atlas of Lithological-Paleogeographical Maps of the World, Mesozoic and Cenozoic of the Continents*. Leningrad, Russ.: Minist. Geol. USSR
- Ronov AB, Khain YE, Slavinsky K. 1984. *Atlas of Lithological-Paleogeographical Maps of the World, Precambrian and Paleozoic of the Continents*. Leningrad, Russ.: Minist. Geol. USSR

- Ross CA, Ross JR. 1985. Late Paleozoic depositional sequences are synchronous and worldwide. *Geology* 13:194–97
- Rowley DB. 1996. Age of initiation of collision between India and Asia: a review of stratigraphic data. *Earth Planet. Sci. Lett.* 145:1–13
- Rowley DB. 1998. Minimum age of initiation of collision between India and Asia north of Everest based on the subsidence history of the Zhepure Mountain section. *J. Geol.* 106:229–35
- Rowley DB. 2017. Earth's constant mean elevation: implication for long-term sea level controlled by oceanic lithosphere dynamics in a Pitman world. *J. Geol.* 125:141–53
- Rowley DB. 2018. Oceanic axial depth and age-depth distribution of oceanic lithosphere: comparison of magnetic anomaly picks versus age-grid models. *Lithosphere* 11(1):21–43
- Rowley DB, Currie BS. 2006. Palaeo-altimetry of the late Eocene to Miocene Lunpola basin, central Tibet. *Nature* 439:677–81
- Rowley DB, Garzione CN. 2007. Stable isotope-based paleoaltimetry. *Annu. Rev. Earth Planet. Sci.* 35:463–508
- Rowley DB, Pierrehumbert RT, Currie BS. 2001. A new approach to stable isotope-based paleoaltimetry: implications for paleoaltimetry and paleohypsometry of the High Himalaya since the Late Miocene. *Earth Planet. Sci. Lett.* 188:253–68
- Schandelmeier H, Reynolds O. 1997. *Palaeogeographic–Palaeotectonic Atlas of North-Eastern Africa, Arabia, and Adjacent Areas: Late Proterozoic to Holocene*. Rotterdam, Neth.: A.A. Balkema
- Scher HD, Martin EE. 2006. Timing and climatic consequences of the opening of Drake Passage. *Science* 312:428–30
- Schlanger SO, Jenkyns HC. 1976. Cretaceous oceanic anoxic events: causes and consequences. *Geol. Mijnb.* 55:179–84
- Sclater JG, Jaupart C, Galson D. 1980. The heat flow through oceanic and continental crust and the heat loss of the Earth. *Rev. Geophys. Space Phys.* 18:269–311
- Scotese CR. 1990. *Atlas of Phanerozoic plate tectonic reconstructions*. PALEOMAP Progress Rep. 01-1090a. Univ. Tex., Arlington, TX
- Scotese CR. 1998. *Digital Paleogeographic map archive on CD-ROM*. PALEOMAP Project, Univ. Tex., Arlington, TX
- Scotese CR. 2001. Animation of Plate Motions and Global Plate Boundary Evolution since the Late Precambrian. *Geol. Soc. Am. Abstr. Programs* 33(6):85
- Scotese CR. 2002. 3D paleogeographic and plate tectonic reconstructions: the PALEOMAP Project is back in town. *Bull. Houston Geolog. Soc.* 44(9):13–15
- Scotese CR. 2004. Cenozoic and Mesozoic paleogeography: changing terrestrial biogeographic pathways. In *Frontiers of Biogeography: New Directions in the Geography of Nature*, ed. MV Lomolino, LH Heaney, pp. 1–26. Sunderland, MA: Sinauer Assoc.
- Scotese CR. 2008a. *The PALEOMAP Project PaleoAtlas for ArcGIS, version 1, Vol. 1, Cenozoic paleogeographic, paleoclimatic and plate tectonic reconstructions*. PALEOMAP Project, Univ. Tex., Arlington, TX
- Scotese CR. 2008b. *The PALEOMAP Project PaleoAtlas for ArcGIS, version 1, Vol. 2, Cretaceous paleogeographic, paleoclimatic and plate tectonic reconstructions*. PALEOMAP Project, Univ. Tex., Arlington, TX
- Scotese CR. 2008c. *The PALEOMAP Project PaleoAtlas for ArcGIS, version 1, Vol. 3, Jurassic paleogeographic, paleoclimatic and plate tectonic reconstructions*. PALEOMAP Project, Univ. Tex., Arlington, TX
- Scotese CR. 2008d. *The PALEOMAP Project PaleoAtlas for ArcGIS, version 1, Vol. 4, Late Paleozoic paleogeographic, paleoclimatic and plate tectonic reconstructions*. PALEOMAP Project, Univ. Tex., Arlington, TX
- Scotese CR. 2008e. *The PALEOMAP Project PaleoAtlas for ArcGIS, version 1, Vol. 5, Early Paleozoic paleogeographic, paleoclimatic and plate tectonic reconstructions*. PALEOMAP Project, Univ. Tex., Arlington, TX
- Scotese CR. 2008f. *The PALEOMAP Project PaleoAtlas for ArcGIS, version 1, Vol. 6, Late Precambrian Paleozoic paleogeographic, paleoclimatic and plate tectonic reconstructions*. PALEOMAP Project, Univ. Tex., Arlington, TX
- Scotese CR. 2009. Late Proterozoic plate tectonics and paleogeography: a tale of two supercontinents, Rodinia and Pannotia, in global Neoproterozoic petroleum systems: the emerging potential in North Africa. *Geol. Soc. Lond. Spec. Pap.* 326:67–83
- Scotese CR. 2014a. *Atlas of Phanerozoic Oceanic Anoxia (Mollweide Projection)*, Vol. 1–6: PALEOMAP Project PaleoAtlas for ArcGIS. Evanston, IL: PALEOMAP Project

- Scotese CR. 2014b. *Atlas of Plate Tectonic Reconstructions (Mollweide Projection)*, Vol. 1–6: PALEOMAP Project *PaleoAtlas for ArcGIS*. Evanston, IL: PALEOMAP Project
- Scotese CR. 2016. *Tutorial: PALEOMAP Paleoatlas for GPlates and the PaleoData Plotter Program*. Tutor, PALEOMAP Project. <http://www.earthbyte.org/paleomap-paleoatlas-for-gplates/>
- Scotese CR. 2017. *Atlas of Oceans & Continents: Plate Tectonics, 1.5 Billion Years-Today*. PALEOMAP Proj. Rep. 112117A, PALEOMAP Project, Evanston, IL. https://www.researchgate.net/publication/321197460_Atlas_of_Ancient_Oceans_Continents_15_billion_years_-_Today
- Scotese CR. 2018. *Plate tectonic evolution during the last 1.5 billion years: the movie*. Paper presented at the Geological Society of America Annual Meeting, Indianapolis, IN, Nov. 5
- Scotese CR, Bambach RJ, Barton C, van der Voo R, Ziegler AM. 1979. Paleozoic base maps. *J. Geol.* 87(3):217–77
- Scotese CR, Boucot AJ, McKerrow WS. 1999. Gondwanan paleogeography and paleoclimatology. *J. Afr. Earth Sci.* 28(1):99–114
- Scotese CR, Dammrose R. 2008. Plate boundary evolution and mantle plume eruptions during the last billion years. *Geol. Soc. Am. Abstr. Programs* 40(6):328
- Scotese CR, McKerrow WS. 1990. Revised world maps and introduction. *Geol. Soc. Lond. Mem.* 12:1–21
- Scotese CR, Moore TL. 2014a. *Atlas of Phanerozoic Ocean Currents and Salinity (Mollweide Projection)*, Vol. 1–6: PALEOMAP Project *PaleoAtlas for ArcGIS*. Evanston, IL: PALEOMAP Project
- Scotese CR, Moore TL. 2014b. *Atlas of Phanerozoic Rainfall (Mollweide Projection)*, Vol. 1–6: PALEOMAP Project *PaleoAtlas for ArcGIS*. Evanston, IL: PALEOMAP Project
- Scotese CR, Moore TL. 2014c. *Atlas of Phanerozoic Temperatures (Mollweide Projection)*, Vol. 1–6: PALEOMAP Project *PaleoAtlas for ArcGIS*. Evanston, IL: PALEOMAP Project
- Scotese CR, Moore TL. 2014d. *Atlas of Phanerozoic Upwelling Zones (Mollweide Projection)*, Vol. 1–6: PALEOMAP Project *PaleoAtlas for ArcGIS*. Evanston, IL: PALEOMAP Project
- Scotese CR, Moore TL. 2014e. *Atlas of Phanerozoic Winds and Atmospheric Pressure (Mollweide Projection)*, Vol. 1–6: PALEOMAP Project *PaleoAtlas for ArcGIS*. Evanston, IL: PALEOMAP Project
- Scotese CR, Sager WW, eds. 1989. *Mesozoic and Cenozoic Plate Reconstructions*. Amsterdam: Elsevier
- Scotese CR, Schettino A. 2017. Late Permian-Early Jurassic paleogeography of Western Tethys and the world. In *Permo-Triassic Salt Provinces of Europe, North Africa and the Atlantic Margins*, ed. JI Soto, J Flinch, G Tari, pp. 57–95. Amsterdam: Elsevier
- Scotese CR, Song H, Mills B, van der Meer D. 2021. Phanerozoic paleotemperatures: the earth's changing climate during the last 540 million years. *Earth-Sci. Rev.* 2021:103503
- Scotese CR, Wright N. 2018. *PALEOMAP Paleodigital Elevation Models (PaleoDEM)* for the Phanerozoic. PaleoDEM, PALEOMAP Project. <https://www.earthbyte.org/paleodem-resource-scotese-and-wright-2018/>
- Şengör AMC, Atayman S. 2009. *The Permian Extinction and the Tethys: An Exercise in Global Geology*. Boulder, CO: Geol. Soc. Am.
- Şengör AMC, Cin A, Rowley DB, Nie SY. 1993. Space-time patterns of magmatism along the Tethysides: a preliminary study. *J. Geol.* 101:51–84
- Şengör AMC, Natal'in BA. 1996. Paleotectonics of Asia: fragments of a synthesis. In *The Tectonic Evolution of Asia*, ed. A Yin, TM Harrison, pp. 486–640. Cambridge, UK: Cambridge Univ. Press
- Şengör AMC, Natal'in BA, Sunal G, van der Voo R. 2014a. A new look at the Altaids: a superorogenic complex in Northern and Central Asia as a factory of continental crust, Part I: geological data compilation (exclusive of paleomagnetic observations). *Austrian J. Earth Sci.* 107(1):169–232
- Şengör AMC, Natal'in BA, van der Voo R, Sunal G. 2014b. A new look at the Altaids: a superorogenic complex in Northern and Central Asia as a factory of continental crust, Part II: palaeomagnetic data, reconstructions, crustal growth, and global sea-level. *Austrian J. Earth Sci.* 107(2):131–81
- Seton M, Müller RD, Zahirovic S, Gaina C, Torsvik TH, et al. 2012. Global continental and ocean basin reconstructions since 200 Ma. *Earth-Sci. Rev.* 113:212–70
- Sheehan PM. 2001. The late Ordovician mass extinction. *Annu. Rev. Earth Planet. Sci.* 29:331–64
- Sheehan PM, Coorough PJ. 1990. Brachiopod zoogeography across the Ordovician-Silurian extinction event. *Geol. Soc. Lond. Mem.* 12:181–87

- Shubin N. 2008. *Your Inner Fish: A Journey into the 3.5 Billion Year History of the Human Body*. New York: Pantheon Books
- Simmons MD. 2012. Sequence stratigraphy and sea-level change. In *The Geologic Time Scale 2012*, ed. FM Gradstein, JG Ogg, M Schmitz, G Ogg, pp. 239–67. Amsterdam: Elsevier
- Smith AG. 1999. Gondwana: its shape, size, position from Cambrian to Triassic times. *J. Afr. Earth Sci.* 28:71–98
- Smith AG, Smith DG, Funnell BM. 1994. *Atlas of Mesozoic and Cenozoic Coastlines*. Cambridge, UK: Cambridge Univ. Press
- Smith W. 1815. *A Delineation of the Strata of England and Wales and Part of Scotland*. London: J. Cary
- Smith WHF, Sandwell DT. 1997. Global sea floor topography from satellite altimetry and ship depth soundings. *Science* 277:1956–62
- Snedden JW, Liu C. 2010. A compilation of Phanerozoic sea-level change, coastal onlaps and recommended sequence designations. *AAPG Search Discov. Artic.* 2010:40594
- Snedden JW, Liu C. 2011. Recommendations for a uniform chronostratigraphic designation system for Phanerozoic depositional sequences. *AAPG Bull.* 95:1095–122
- Stampfli GM. 2000. Tethyan oceans. *Geol. Soc. Lond. Spec. Publ.* 173:1–23
- Stampfli GM, Borel GD. 2002. A plate tectonic model for the Paleozoic and Mesozoic constrained by dynamic plate boundaries and restored synthetic oceanic isochrons. *Earth Planet. Sci. Lett.* 196:17–33
- Stampfli GM, Borel GD. 2004. The TRANSMED transects in space and time: constraints on the paleotectonic evolution of the Mediterranean domain. In *The TRANSMED Atlas: The Mediterranean Region from Crust to Mantle*, ed. W Cavazza, FM Roura, W Spakman, GM Stampfli, PA Ziegler, pp. 53–80. Berlin: Springer
- Stampfli GM, Hochard C, Verard C, Wilhe C, von Raumer J. 2013. The formation of Pangea. *Tectonophysics* 593:1–19
- Stampfli GM, Kozur HW. 2006. Europe from the Variscan to the Alpine cycles. In *European Lithosphere Dynamics*, ed. DG Gee, RA Stephenson, pp. 57–82, London: Geol. Soc. Lond.
- Stampfli GM, Mosar J, Favre PH, Pillevuit A, Vannay JC. 2001. Permo-Mesozoic evolution of the western Tethys realm: the Neo-Tethys East Mediterranean Basin connection. See Ziegler et al. 2001, pp. 51–108
- Stampfli GM, Pillevuit A. 1993. An alternative Permo-Triassic reconstruction of the kinematics of the Tethyan realm. See Dercourt et al. 1993, pp. 9–20
- Stein CA, Stein S. 1992. A model for the global variation in oceanic depth and heat flow with lithospheric age. *Nature* 359:123–29
- Steininger FF, Wessley G. 2000. From the Tethyan Ocean to the Paratethys Sea: Oligocene to Neogene stratigraphy, paleogeography and paleobiogeography of the circum-Mediterranean region and the Oligocene to Neogene Basin evolution in Austria. *Mitt. Osterr. Geol. Ges.* 92:95–116
- Stern RJ. 1994. Arc assembly and continental collision in the Neoproterozoic East Africa Orogen: implications for the consolidation of Gondwanaland. *Annu. Rev. Earth Planet. Sci.* 33:319–51
- Swanson-Hysell NL, Macdonald FA. 2017. Tropical weathering of the Taconic Orogeny as a driver for Ordovician cooling. *Geology* 45:719–22
- Tabor NJ, DiMechele WA, Montañez IP, Chaney DS. 2013. Late Paleozoic continental warming of a cold tropical basin and floristic change in western Pangea. *Int. J. Coal Geol.* 119:177–86
- Toggweiler JR, Bjornsson H. 2000. Drake Passage and palaeoclimate. *J. Quat. Sci.* 15:319–28
- Torsvik TH, Cocks LRM. 2017. *Earth History and Palaeogeography*. Cambridge, UK: Cambridge Univ. Press
- Trotter JA, Williams IS, Barnes CR, LeCuyer C, Nicoll RS. 2008. Did cooling oceans trigger Ordovician biodiversification? Evidence from conodont thermometry. *Science* 321(5888):550–54
- Ulmishek GF, Klemme HD. 1990. Depositional controls, distribution, and effectiveness of the world's petroleum source rocks. *USGS Bull.* 1931:59
- Vail PR, Mitchum RM, Todd RG, Widmier JM, Thompson S III, et al. 1977. Seismic stratigraphy and global changes in sea level. In *Seismic Stratigraphy—Applications to Hydrocarbon Exploration*, ed. CE Payton, pp. 49–212. Tulsa, OK: Am. Assoc. Pet. Geol.
- Valdes PJ, Scotese CR, Lunt DJ. 2018. *Modelling the Climate History of the Phanerozoic, Toward a Phanerozoic History of the Earth's Surface Temperature*. Poster presented at the American Geophysical Union Centennial Meeting, Washington, DC, Dec. 10

- van der Linden TJM, Dupont-Nivet G, van Hinsbergen DJJ. 2020. *Towards a quantitative paleogeography calculator*. Presented at EGU General Assembly, online, May 8
- van der Meer DG, van den Berg X, van Saparoea APH, Hinsbergen DJJ, van de Weg RMB, et al. 2017. Reconstructing first-order changes in sea level during the Phanerozoic and Neoproterozoic using strontium isotopes. *Gondwana Res.* 44:22–34
- van der Voo R. 1993. *Paleomagnetism of the Atlantic, Tethys, and Iapetus Oceans*. Cambridge, UK: Cambridge Univ. Press
- Veevers JJ. 1984. *Phanerozoic Earth History of Australia*. New York: Oxford Univ. Press
- Veevers JJ. 2000. *Billion-Year History of Australia and Neighbours in Gondwanaland*. Sydney: GEMOC
- Verard C. 2019. Panalysis: towards global synthetic paleogeographies using integration and coupling manifold models. *Geol. Mag.* 156(2):320–30
- Verard C, Hochard C, Baumgartner O, Stampfli GM. 2015. 3D palaeogeographic reconstructions of the Phanerozoic versus sea-level and Sr-ratio variations. *J. Palaeogeogr.* 4(1):64–84
- Vinogradov AP, Vereshchagin VN, Nalivkin VD, Ronov AB, Khabakov AV, Khain VE. 1967. *Atlas of Lithological-Paleogeographical Maps of the U.S.S.R. (1:7.500,00)*, Tome IV, Paleogene, Neogene, and Quaternary, ed. VA Grossheim, VE Khain. Moscow: Acad. Sci. USSR
- Vinogradov AP, Vereshchagin VN, Nalivkin VD, Ronov AB, Khabakov AV, Khain VE. 1968a. *Atlas of Lithological-Paleogeographical Maps of the U.S.S.R. (1:7.500,00)*, Tome I, Precambrian, Cambrian, Ordovician, and Silurian, ed. BM Keller, NN Predtechensky. Moscow: Acad. Sci. USSR
- Vinogradov AP, Vereshchagin VN, Nalivkin VD, Ronov AB, Khabakov AV, Khain VE. 1968b. *Atlas of Lithological-Paleogeographical Maps of the U.S.S.R. (1:7.500,00)*, Tome III, Triassic, Jurassic, and Cretaceous, ed. VN Vereshchagin, AB Ronov. Moscow: Acad. Sci. USSR
- Vinogradov AP, Vereshchagin VN, Nalivkin VD, Ronov AB, Khabakov AV, Khain VE. 1969. *Atlas of Lithological-Paleogeographical Maps of the U.S.S.R. (1:7.500,00)*, Tome II, Devonian, Carboniferous, and Permian, ed. VD Nalivkin, VM Posner. Moscow: Acad. Sci. USSR
- Wang H. 1985. *Atlas of the Paleogeography of China*. Beijing: Cartogr. Publ. House
- Xiao W, Kröner A, Windley B. 2009. Geodynamic evolution of Central Asia in the Paleozoic and Mesozoic. *Int. J. Earth Sci.* 98:1185–88
- Yilmaz O, Norton IO, Leary D, Chuchla RJ. 1996. Tectonic evolution and paleogeography of Europe. See Ziegler & Horvath 1996, pp. 47–60, encl. 1–13
- Young A, Flament N, Maloney K, Williams S, Matthews K, et al. 2019. Global kinematics of tectonic plates and subduction zones since the late Paleozoic Era. *Geosci. Front.* 10:989–1013
- Zheng HR, Hu ZQ, eds. 2010. *Atlas of Pre-Mesozoic Tectonic Lithofacies Paleogeography in China*. Beijing: Geol. Publ. House
- Ziegler AM. 1975. *A proposal to produce an atlas of paleogeographic maps*. Rep. Dep. Geophys. Sci., Univ. Chicago
- Ziegler AM, Hansen KS, Johnson ME, Kelly MA, Scotese CR, van der Voo R. 1977. Silurian continental distributions, paleogeography, climatology, and biogeography. *Tectonophysics* 40:13–51
- Ziegler AM, Hulver ML, Rowley DB. 1997. Permian world topography and climate. In *Late Glacial and Post-glacial Environmental Changes: Quaternary, Carboniferous-Permian and Proterozoic*, ed. I Martini, pp. 111–46. New York: Oxford Univ. Press
- Ziegler AM, Rowley DB, Lottes AL, Sahagian DL, Hulver ML, Gierlowski TC. 1985. Paleogeographic interpretation: with an example from the Mid-Cretaceous. *Annu. Rev. Earth Planet. Sci.* 13:385–425
- Ziegler AM, Scotese CR. 1977. *Thoughts on format for the forthcoming “Atlas of Paleogeographic Maps.”* Tech. Rep. Dep. Geophys. Sci., Univ. Chicago
- Ziegler AM, Scotese CR, Barrett SF. 1983. Mesozoic and Cenozoic paleogeographic maps. In *Tidal Friction and the Earth’s Rotation II*, ed. P Broche, J Sundermann, pp. 241–52. Berlin: Springer-Verlag
- Ziegler AM, Scotese CR, McKerrow WS, Johnson ME, Bambach RK. 1979. Paleozoic paleogeography. *Annu. Rev. Earth Planet. Sci.* 7:473–502
- Ziegler PA. 1982. *Geological Atlas of Western and Central Europe*. Den Haag: Shell Int. Pet. Maatsch.
- Ziegler PA. 1988. *Evolution of Arctic-North Atlantic and Western Tethys*. Tulsa, OK: Am. Assoc. Pet. Geol.
- Ziegler PA. 1989. *Evolution of Laurussia: A Study in Late Paleozoic Plate Tectonics*. Dordrecht, Neth.: Kluwer
- Ziegler PA. 1990. *Geological Atlas of Western and Central Europe*. Den Haag: Shell Int. Pet. Maatsch.

- Ziegler PA, Cavazza W, Robertson AHF, Crasquin-Soleau S, eds. 2001. *Tethys Memoir, 6: Peri-Tethyan Rift/Wrench Basins and Passive Margins*. Paris: Éd. Mus. Natl. Hist. Nat.
- Ziegler PA, Horvath F, eds. 1996. *A Peri-Tethys Memoir, 2: Structure and Prospects of Alpine Basins and Forelands*. Paris: Éd. Mus. Natl. Hist. Nat.
- Zonenshain LP, Kuzmin MI, Natapov LM. 1990. *Geology of the USSR: A Plate Tectonic Synthesis*. Washington, DC: Am. Geophys. Union

Contents

Minoru Ozima: Autobiographical Notes

Minoru Ozima 1

The Geodynamic Evolution of Iran

Robert J. Stern, Hadi Shafaii Moghadam, Mortaza Pirouz, and Walter Mooney 9

Subduction-Driven Volatile Recycling: A Global Mass Balance

D.V. Bekaert, S.J. Turner, M.W. Broadley, J.D. Barnes, S.A. Halldórsson, J. Labidi, J. Wade, K.J. Walowski, and P.H. Barry 37

Atmospheric Loss to Space and the History of Water on Mars

Bruce M. Jakosky 71

Climate Risk Management

Klaus Keller, Casey Helgeson, and Vivek Srikrishnan 95

Continental Drift with Deep Cratonic Roots

Masaki Yoshida and Kazunori Yoshizawa 117

Contemporary Liquid Water on Mars?

James J. Wray 141

Geologically Diverse Pluto and Charon: Implications for the Dwarf

Planets of the Kuiper Belt

Jeffrey M. Moore and William B. McKinnon 173

The Laurentian Great Lakes: A Biogeochemical Test Bed

Robert W. Stern 201

Clocks in Magmatic Rocks

Fidel Costa 231

Hydration and Dehydration in Earth's Interior

Eiji Ohtani 253

Past Warmth and Its Impacts During the Holocene Thermal

Maximum in Greenland

Yarrow Axford, Anne de Vernal, and Erich C. Osterberg 279

Fiber-Optic Seismology

Nathaniel J. Lindsey and Eileen R. Martin 309

Earth's First Redox Revolution

Chadlin M. Ostrander, Aleisha C. Johnson, and Ariel D. Anbar 337

Toward an Integrative Geological and Geophysical View of Cascadia Subduction Zone Earthquakes	
<i>Maureen A.L. Walton, Lydia M. Staisch, Tina Dura, Jessie K. Pearl, Brian Sherrod, Joan Gomberg, Simon Engelhart, Anne Tréhu, Janet Watt, Jon Perkins, Robert C. Witter, Noel Bartlow, Chris Goldfinger, Harvey Kelsey, Ann E. Morey, Valerie J. Sahakian, Harold Tobin, Kelin Wang, Ray Wells, and Erin Wirth</i>	367
Recent Advances in Geochemical Paleo-Oxybarometers	
<i>Brian Kendall</i>	399
The Organic Isotopologue Frontier	
<i>Alexis Gilbert</i>	435
Olivine-Hosted Melt Inclusions: A Microscopic Perspective on a Complex Magmatic World	
<i>Paul J. Wallace, Terry Plank, Robert J. Bodnar, Glenn A. Gaetani, and Thomas Shea</i>	465
Architectural and Tectonic Control on the Segmentation of the Central American Volcanic Arc	
<i>Esteban Gazel, Kennet E. Flores, and Michael J. Carr</i>	495
Reactive Nitrogen Cycling in the Atmosphere and Ocean	
<i>Katye E. Altieri, Sarah E. Fawcett, and Meredith G. Hastings</i>	523
Submarine Landslides and Their Tsunami Hazard	
<i>David R. Tappin</i>	551
Titan's Interior Structure and Dynamics After the Cassini-Huygens Mission	
<i>Christophe Sotin, Klára Kalousová, and Gabriel Tobie</i>	579
Atmospheric CO ₂ over the Past 66 Million Years from Marine Archives	
<i>James W.B. Rae, Yi Ge Zhang, Xiaoqing Liu, Gavin L. Foster, Heather M. Stoll, and Ross D.M. Whiteford</i>	609
A 2020 Observational Perspective of Io	
<i>Imke de Pater, James T. Keane, Katherine de Kleer, and Ashley Gerard Davies</i>	643
An Atlas of Phanerozoic Paleogeographic Maps: The Seas Come In and the Seas Go Out	
<i>Christopher R. Scotese</i>	679

Errata

An online log of corrections to *Annual Review of Earth and Planetary Sciences* articles may be found at <http://www.annualreviews.org/errata/earth>

Related Articles

From the *Annual Review of Astronomy and Astrophysics*, Volume 58 (2020)

Observations of Protoplanetary Disk Structures

Sean M. Andrews

Astrochemistry During the Formation of Stars

Jes K. Jørgensen, Arnaud Belloche, and Robin T. Garrod

From the *Annual Review of Ecology, Evolution, and Systematics*, Volume 51 (2020)

Arthropod Origins: Integrating Paleontological and Molecular Evidence

Gregory D. Edgecombe

Origin and Evolution of the Turtle Body Plan

Tyler R. Lyson and Gabriel S. Bever

From the *Annual Review of Environment and Resources*, Volume 45 (2020)

Soil Microbiomes Under Climate Change and Implications for Carbon Cycling

Dan Naylor, Natalie Sadler, Arunima Bhattacharjee, Emily B. Graham,

Christopher R. Anderton, Ryan McClure, Mary Lipton,

Kirsten S. Hofmockel, and Janet K. Jansson

From the *Annual Review of Fluid Mechanics*, Volume 53 (2021)

Turbulence Processes Within Turbidity Currents

Mathew G. Wells and Robert M. Dorrell

Statistics of Extreme Events in Fluid Flows and Waves

Themistoklis P. Sapsis

Layering, Instabilities, and Mixing in Turbulent Stratified Flows

C.P. Caulfield

Mixing by Oceanic Lee Waves

Sonya Legg

From the *Annual Review of Marine Science*, Volume 13 (2021)

Right Place, Right Time: An Informal Memoir

Carl Wunsch

The Dissolution Rate of CaCO₃ in the Ocean

*Jess F. Adkins, John D. Navaux, Adam V. Subbas, Sijia Dong,
and William M. Berelson*

The Complexity of Spills: The Fate of the *Deepwater Horizon* Oil

Uta Passow and Edward B. Overton

New Microbial Biodiversity in Marine Sediments

Brett J. Baker, Kathryn E. Appler, and Xianzhe Gong

Variations in Ocean Mixing from Seconds to Years

James N. Moum

Combining Modern and Paleoceanographic Perspectives on Ocean Heat Uptake

Geoffrey Gebbie

Historical Estimates of Surface Marine Temperatures

Elizabeth C. Kent and John J. Kennedy

Turbulence and Coral Reefs

Kristen A. Davis, Geno Pawlak, and Stephen G. Monismith

Amazon Sediment Transport and Accumulation Along the Continuum of Mixed Fluvial and Marine Processes

*Charles A. Nittrouer, David J. DeMaster, Steven A. Kuehl, Alberto G. Figueiredo Jr.,
Richard W. Sternberg, L. Ercilio C. Faria, Odete M. Silveira, Mead A. Allison,
Gail C. Kineke, Andrea S. Ogston, Pedro W.M. Souza Filho, Nils E. Asp,
Daniel J. Nowacki, and Aaron T. Fricke*

The Origin of Modern Atolls: Challenging Darwin's Deeply Ingrained Theory

André W. Droxler and Stéphan J. Jorry

From the *Annual Review of Materials Research*, Volume 50 (2020)

Antisymmetry: Fundamentals and Applications

Hari Padmanabhan, Jason M. Munro, Ismaila Dabo, and Venkatraman Gopalan

Noble Metal Nanomaterials with Nontraditional Crystal Structures

Chaitali Sow, Suchithra P, Gangaiah Mettela, and Giridhar U. Kulkarni

High-Energy X-Ray Diffraction Microscopy in Materials Science

Joel V. Bernier, Robert M. Suter, Anthony D. Rollett, and Jonathan D. Almer

Frontiers in the Simulation of Dislocations

Nicolas Bertin, Ryan B. Sills, and Wei Cai

Grain Boundary Complexion Transitions

*Patrick R. Cantwell, Timofey Frolov, Timothy J. Rupert, Amanda R. Krause,
Christopher J. Marvel, Gregory S. Rohrer, Jeffrey M. Rickman,
and Martin P. Harmer*